A SCANNING ELECTRON MICROSCOPE STUDY OF THE EFFECTS OF ANODE VELOCITY AND CURRENT DENSITY ON THE CORROSION OF SHIP HULL ZINC IN SYNTHETIC SEAWATER

William Howard Luebke

NAVAL POSTGRADUATE SCHOOL
Monterey, California

THESIS

A SCANNING ELECTRON MICROSCOPE STUDY
OF THE EFFECTS OF ANODE VELOCITY
AND CURRENT DENSITY ON THE CORROSION OF
SHIP HULL ZINC IN SYNTHETIC SEAWATER

by

William Howard Luebke

June 1976

Thesis Advisor: A. J. Perkins

SECURITY CLASSIFICATION OF THIS PAGE (When Data Entered)

REPORT DOCUMENTATION PAGE

READ INSTRUCTIONS BEFORE COMPLETING FORM

1. REPORT NUMBER

2. GOVT ACCESSION NO.

3. RECIPIENT'S CATALOG NUMBER

4. TITLE (and Subtitle)
A Scanning Electron Microscope Study of the Effects of Anode Velocity and Current Density on the Corrosion of Ship Hill Zinc in Synthetic Seawater

5. TYPE OF REPORT & PERIOD COVERED
Master's Thesis
June 1976

6. PERFORMING ORG. REPORT NUMBER

7. AUTHOR(s)
William Howard Luebke

8. CONTRACT OR GRANT NUMBER(s)

9. PERFORMING ORGANIZATION NAME AND ADDRESS
Naval Postgraduate School
Monterey, California 93940

10. PROGRAM ELEMENT, PROJECT, TASK AREA & WORK UNIT NUMBERS

11. CONTROLLING OFFICE NAME AND ADDRESS
Naval Postgraduate School
Monterey, California 93940

12. REPORT DATE
June 1976

13. NUMBER OF PAGES
168

14. MONITORING AGENCY NAME & ADDRESS(if different from Controlling Office)
Naval Postgraduate School
Monterey, California 93940

15. SECURITY CLASS. (of this report)
Unclassified

15a. DECLASSIFICATION/DOWNGRADING SCHEDULE

16. DISTRIBUTION STATEMENT (of this Report)
Approved for public release; distribution unlimited.

17. DISTRIBUTION STATEMENT (of the abstract entered in Block 20, if different from Report)

18. SUPPLEMENTARY NOTES

19. KEY WORDS (Continue on reverse side if necessary and identify by block number)

20. ABSTRACT (Continue on reverse side if necessary and identify by block number)

The structure of corrosion products formed on anodic ship hull zinc due to impressed current in synthetic seawater electrolyte was studied as a function of anode velocity, current density, and current-time product. Under dynamic situations, corrosion product growth is discussed for a variety of current densities, and a model is developed considering hydrodynamic and diffusion boundary layer effects on electrical double

DD FORM 1 JAN 73 1473 EDITION OF 1 NOV 65 IS OBSOLETE
S/N 0102-014-6601 |
(Page 1)

SECURITY CLASSIFICATION OF THIS PAGE (When Data Entered)

layer stability. Conditions leading to the formation of various corrosion product types are defined and their development with time is followed. The effects of various velocities, current densities, and current-time products on the development of ZnO platelet networks, ribbonlike corrosion products, and anodic passivation layers are analyzed in static and dynamic environments and models for the sequential observations are developed. A model controlled by current density is offered for static conditions at low and moderate current densities, leading to either non-passivating network layers or compact passivating layers depending on the conditions. A corrosion product growth/removal cycle is hypothesized for very-high current density/high velocity situations which does not lead to zinc anode passivation.

A Scanning Electron Microscope Study of the Effects of Anode Velocity and Current Density on the Corrosion of Ship Hull Zinc in Synthetic Seawater

by

William Howard Luebke
Ensign, United States Navy
B. S., United States Naval Academy, 1975

Submitted in partial fulfillment of the requirements for the degree of

MASTER OF SCIENCE IN MECHANICAL ENGINEERING

from the

NAVAL POSTGRADUATE SCHOOL
June 1976

ABSTRACT

The structure of corrosion products formed on anodic ship hull zinc due to impressed current in synthetic seawater electrolyte was studied as a function of anode velocity, current density, and current-time product. Under dynamic situations, corrosion product growth is discussed for a variety of current densities, and a model is developed considering hydrodynamic and diffusion boundary layer effects on electrical double layer stability. Conditions leading to the formation of various corrosion product types are defined and their development with time is followed. The effects of various velocities, current densities, and current-time products on the development of ZnO platelet networks, ribbonlike corrosion products, and anodic passivation layers are analyzed in static and dynamic environments and models for the sequential observations are developed. A model controlled by current density is offered for static conditions at low and moderate current densities, leading to either non-passivating network layers or compact passivating layers depending on the conditions. A corrosion product growth/removal cycle is hypothesized for very-high current density/high velocity situations which does not lead to zinc anode passivation.

TABLE OF CONTENTS

LIST OF TABLES

LIST OF FIGURES

LIST OF SYMBOLS

A	Arrhenius constant
a_{H^+}	hydrogen ion activity
a_Q^q, a_R^r, etc.	elemental ionic activities
Al	aluminum
Br^-	bromine ion
°C	degrees Celsius
Ca^{++}	calcium ion
$CaCl_2$	calcium chloride
Cl^-	chlorine ion
cm	centimeter
cm^2	square centimeter
__°	degrees of arc
δ	diffusion boundary layer thickness
δ_o	hydrodynamic boundary layer thickness
D.C.	direct current
E	electrode potential
E^o	standard reference potential
e^-	electron
emf	electromotive force
exp	base of natural logarithms
F	Faraday constant (96,500 coulombs)
F^-	fluorine ion
°F	degrees Fahrenheit

Fe	iron
Fe_2Al_5	iron aluminide
FeSi	iron silicide
fps	feet per second
ft	feet
ft^2	square feet
g	gram
H_2	hydrogen
H^+	hydrogen ion
H_3BO_3	boric acid
HCO_3^-	hydrogen carbonate ion
H_2O	water
hr(s)	hour(s)
in	inch
in^2	square inch
K^+	potassium ion
KBr	potassium bromide
KCl	potassium chloride
kg	kilogram
kV	kilovolt
l	liter
LED	light emitting diode
Li	lithium
ln	natural logarithm
log	logarithm (base 10)
M	metal
M^+	metal ion

$\dot{M}$	mole
m	meter
m^2	square meter
mA	milliamp
M.F.D.	microfarad
Mg^{++}	magnesium ion
$MgCl_2$	magnesium chloride
min	minute
ml	milliliter
mmho	millimho
μm	micrometer
m/s	meters per second
n	number of electrons in cell reaction (faraday/mole)
Na^+	sodium ion
NaCl	sodium chloride
NaF	sodium fluoride
$NaHCO_3$	sodium carbonate
Na_2SO_4	sodium sulfate
Ω	ohm
O_2	oxygen
OH^-	hydroxide ion
Pb	lead
pH	standard hydrogen potential ($pH = -\log a_{H^+}$)
ppm	parts per million
Pr	Prandtl number (diffusion)

Q	activation energy
R	universal gas constant (8.314 joules/degree•mole)
$\dot{R}$	resistance
rpm	revolutions per minute
SEM	scanning electron microscope
Si	silicon
SO_4^{--}	sulfate ion
Sr^{--}	strontium ion
$SrCl_2$	strontium chloride
T	temperature
U	corrosion rate
VCCG	voltage controlled current generator
VCVG	voltage controlled voltage generator
Zn	zinc
Zn^{++}	zinc ion
$ZnCl_2$	zinc chloride
$ZnCO_3$	zinc carbonate
ZnO	zinc oxide

ACKNOWLEDGEMENT

The author wishes to express his sincere gratitude for assistance from Professor Jeff Perkins, as both friend and advisor, throughout the course of this study. His suggestions during the final editing phase were especially helpful toward the development of a clear and concise manuscript with which to efficiently convey significant results from the undertaking.

Numerous consultations with Professor Turgut Sarpkaya helped to shed light on several perplexing fluid dynamics problems.

Material Science Laboratory Technician, Roy Edwards, deserves a word of thanks for his untiring devotion to upkeep of microscopy equipment and for photographs of the experimental apparatus. Mechanical Engineering Department Technician, George Bixler, warrants praise for quality in construction of the exposure tank assembly from the author's set of drawings while technician Tom Christian designed and built the current/voltage generator necessary for corrosion experiments.

Last but certainly not least, the author is indebted to his loving wife-to-be, Ann, for her unsurpassed encouragement and moral support from afar.

I. INTRODUCTION

A. CATHODIC PROTECTION

Corrosion can be generally defined as a chemical or electrochemical process by which a metal is attacked in its environment. The types of corrosion that have been defined and studied are far too numerous and lengthy to be included as background discussion here and in most cases would shed no light on the topic of interest. Consequently, coverage of one aspect of the electrochemical nature of corrosion to explain the cathodic protection phenomenon will suffice for introductory treatment. In view of the impetus for this study, a compendium of contemporary cathodic protection techniques is included.

By definition, an electrochemical process involves the flow of current through which the chemical character of a substance is modified. Electrical theory in turn states that current can only pass between two points of unequal potential, providing that they are connected by a conductive path. In nature, each elemental reduction reaction stands at a different, identifiable potential (relative to a standard) so that under the proper conditions, two metals will undergo electrochemical corrosion. The occurrence of such a response between two metals coupled in an electrolytic (conductive) solution such as seawater constitutes the existence of a galvanic cell. Here current can flow from one metal to the other via the conductive connection (possibly a

wire) and return to the original metal, via passage through the solution, to complete the circuit. This particular arrangement is the basic mechanism inherent to all cathodic protection concepts.

Given two dissimilar metals in a galvanic cell, and barring unusual circumstances, the amount of current that will initially flow between them as well as its direction is determined by their difference in potential, i.e., the electromotive force (emf) of the corrosion cell. The direction of this force basically decides which of the two will corrode and its magnitude the extent or rate of the selective corrosion. (Here positive current flow implies a direction opposite the flow of electrons.) The metal experiencing electrochemical attack is defined as the anode and is the electrode where positive current flows out into the electrolytic solution path toward the remaining electrode, the cathode. The anodic metal is said to be "oxidized" and the cathodic metal "reduced".

A cell's electromotive force is logically the algebraic sum of its electrode potentials. The well known Nernst equation [1]:

$$E = E^{o} - \frac{RT}{nF} \ln \frac{a_{Q}^{q} \cdot a_{R}^{r} \cdot}{a_{L}^{l} \cdot a_{M}^{m} \cdot}$$

is used to calculate the potential of each electrode and ultimately the emf of the cell. Oxidation of an anode can be shown symbolically as:

$$M \rightarrow M^{+} + e^{-}$$

where M is the metal dissolved. The resulting metal ions

enter into solution and aid electrical conduction. The corresponding reaction for anodic zinc is:

$$Zn \rightarrow Zn^{++} + 2e^{-} .$$

Several possible reactions may constitute the reduction processes at the cathode. In acidic solutions:

$$2H^{+} + 2e^{-} \rightarrow H_2 , \quad \text{or}$$
$$O_2 + 4H^{+} + 4e^{-} \rightarrow H_2O ,$$

while in alkaline or neutral solutions:

$$O_2 + 2H_2O + 4e^{-} \rightarrow 4OH^{-}$$

[2]. The rate of the reduction has been shown to be dependent on the oxygen content of the cathodic environment.

Aside from the natural potential dissimilarities among different metals, it is possible to simultaneously obtain anodic and cathodic regions on the surface of a single metal. Variations in the local environment, i.e., the temperature or oxygen content, and changes in the material's composition or microstructure are common causes of the phenomenon. Some reflection at this point reveals that whatever the situation, the material needing protection must inevitably be made the cathodic electrode when a galvanic cell exists and thus it must be ensured that the emf is conducive to this arrangement. In essence then, cathodic protection is the selective corrosion of an expendable material (anode) for an indispensable material (cathode).

Historically, cathodic protection techniques date back to 1824 when Sir Humphrey Davy found that zinc could be used to protect copper sheathing placed on the hulls of wooden ships [3]. In 1829, Davy's cousin, Edmund, similarly demonstrated that zinc was capable of preserving the iron work of buoys, and in 1840, Robert Mallet created a zinc alloy that improved protection capabilities [1]. As steel hulls were adopted, use of zinc slabs became commonplace, especially near a ship's stern region where bronze propellers created a natural galvanic couple with the hull. After 1900, cathodic protection principles were also applied to submarines, water tanks, stationary steel structures such as piers, and underground pipelines.

The 1940's brought renewed interest in the traditional use of zinc on ships when it was realized that many of the anodes had prematurely ceased to function, leading only to localized shipboard protection. A dense adherent layer of corrosion products on numerous zinc surfaces had prevented them from supplying an adequate protective potential. Extensive investigation disclosed that performance was dependent on certain trace elements commonly found in the zincs. In 1956, Teel and Anderson concluded that the major trace contaminant to zinc anodes was iron and recommended that its content be kept below 0.0015% [4]. Stemming partly from this research, the Navy's Military Specification A-18001H currently limits the maximum iron content of contemporary shipboard zincs [5].

Today, cathodic protection of ships includes the use of zinc, magnesium, and aluminum anodes, as well as impressed current systems. The latter method eliminates the need of a more electronegative material and instead, employs an outside current source to oppose the natural potential of the galvanic cell. Ideally, an equal and opposite emf applied to the basic cell must be developed but experience has indicated that local environmental effects, metallic impurities, and the like, distributed over the hull surface, demand a slightly larger countering current.

The economic benefits of cathodic protection, compared to sole reliance on protective coatings, was demonstrated in a study by Francis and Cook [6]. Experiments performed on actual ships projected average savings of $30,000.00 (1976 $) per destroyer-sized ship per two-year overhaul cycle using sacrificial anodes.

Almost 90% of current United States naval vessels use a zinc protection system. Commonly, 22 pound (48.51 kg) zinc slabs, measuring 6 in x 12 in x 1¼ in (15.24 cm x 30.48 cm x 3.175 cm) and containing galvanized embedded straps for attachment, are welded to each ship's hull-one slab per 100 ft^2 (9.29 m^2) of underwater area. Zinc distribution is dependent upon ship size, shape, and operational environment, and replacement of the anodes can be planned to coincide with an overhaul cycle. Longer time intervals between maintenance work logically demand that more zinc be attached during each upkeep. Conforming to the current three-year restoration

cycle, sufficient slabs to initially deliver a current density of 3.9 mA/ft^2 (0.362 mA/m^2) are required. Two and four year cycles would necessitate initial densities of 2.6 mA/ft^2 (0.242 mA/m^2) and 5.2 mA/ft^2 (0.483 mA/m^2) respectively [7]. Anodic zinc efficiency in seawater is greater than 90%.

Magnesium is even more electronegative than zinc, but its use to date in cathodic protection systems has been limited. The high activity of the metal requires that it be replaced more frequently than zinc and also demands the use of a dielectric shield under each anode. Dielectric shields, generally 2 ft (61 cm) in diameter, protect the surrounding paint from damage which is caused by the evolution of hydrogen gas as a result of the relatively large cathodic current density. (Note the corresponding equation for the cathodic reduction process listed above.) Possible hydrogen embrittlement of high strength steel hulls is a second consideration for use of the dielectric shield. Finally, due to only a 50% efficiency in seawater, magnesium is currently twice as expensive as zinc to replace for a given cathodic protection requirement.

Pending future developments, the use of aluminum as a sacrificial anode could become the predominant form of cathodic protection. Numerous advantages associated with its use have been demonstrated due to its light weight. At 95% efficiency in seawater, aluminum can provide approximately three times the current per equal weight of zinc. Its current output per unit anode area is identical to zinc. These two factors suggest that a six-year aluminum system could be designed that

would be equal in weight to a three-year zinc cycle [7]. Unfortunately, the performance of aluminum anodes is still highly erratic, depending on variations in grain size, heat treatment, and trace impurities. The addition of a small amount of mercury seems to stabilize its performance, but the environmental impact of such an additive has yet to be assessed.

Impressed current cathodic protection systems have been of practical use in the fleet since the 1960's. More complicated than galvanic anodes, a typical system consists of seven basic components: a power source, controller, stuffing glands, cabling, anode material, dielectric shielding, and a reference electrode. Several power supplies are available, all of which ultimately deliver direct current to the controller. Two types of controllers exist, a transistorized, solid-state apparatus and a magnetic model. The latter is preferred due to its dependability and repairability. Either type may be automatically or manually operated. Manual models find use aboard inactive reserve vessels where the cathodic protection requirements remain essentially fixed while automated controllers are required on active crafts to ensure protection in a continually changing environment. Stuffing glands allow hull penetrations by the cabling for connections between the anodic material and controller.

A wide selection of impressed current anodes includes graphite, steel, duriron, lead-silver, lead-platinum, platinized titanium, platinum-paladium, and platinum clad tantalum configurations [7]. Platinum-tantalum is presently preferred,

and has been used aboard ships with few failures and little anode deterioration over a projected 20-year period. Dielectric shields provide more uniform current distribution at acceptable current densities and avoid short circuits. Their diameter is dependent on the type of hull coating and presently shields 5 ft (1.52 m) in diameter are used in conjunction with naval epoxy paints.

The silver/silver-chloride reference electrode is used to determine a system's current requirements by allowing the controller to compare actual hull potential to the desired potential. An inherently low temperature coefficient and average six-year replacement cycle add to this electrode's acceptance over copper/copper-sulfate and zinc models.

The advantages and disadvantages of a sacrificial anode system over an impressed current system are numerous, and proper choice of a particular method requires consideration of many factors in both technical and economic arenas. Proponents of the galvanic approach justifiably argue that an impressed current arrangement is dependent upon an external power supply and that the entire system is subject to mechanical and/or electrical failure. Secondly, its installation is considerably more complicated in that it requires wiring through fuel and water tanks and finally several hull penetrations, resulting in a complex quality control problem. Also, dielectric shields are always required. Finally, the impressed current system is relatively more expensive when used in protecting small to moderately-sized vessels.

Several features of impressed current mechanisms are attractive. They provide broad military flexibility as to hull maintenance requirements, thus eliminating current three-year anode replacement cycles. Underwater anode projections are fewer and more streamlined which minimize ship drag and propulsive power consumption. Finally, adequate protection per unit area of hull, over a 20 year period, can be provided at slightly less than one-third the weight and a little more than one-half the cost of today's sacrificial zinc cycle [7]. Obviously, these tradeoffs can continue to support concurrent use of both methods in the fleet.

B. CORROSION VARIABLES

To date, little research concerning galvanic zinc corrosion has been undertaken which examines the effects of important variables, inherent to any electrochemical activity, via scanning electron miscroscopy. A major goal of this work has been to investigate the microscale results of various combinations of velocity and current density on the formation and morphology of anodic zinc corrosion products.

Electrochemical corrosion, by its very nature, is highly dependent upon many factors. The types of corrosion, corrosion rates, corrosion products, and in fact the basic processes themselves, are governed by the metallic elements involved, the form in which they are present, and the local environment. In addition, as corrosion progresses, some or all of the factors may be altered so that new conditions continue to evolve. Any study dealing with this phenomenon must

account for the substantial impact such factors can have and consequently, efforts to control them are of paramount importance in obtaining valid results.

It is convenient to classify corrosion variables as either internal or external in nature [8]. The former term denotes those properties inherent to the metallic element(s) involved while the latter characterizes significant environmental factors. Among internal considerations affecting corrosion, the following will be discussed briefly: basic thermodynamic feasibility, solid solution stability, metallic structure and surface condition, and mechanical factors. A succinct treatment of external variables includes: electrolyte pH, solution salt concentration, corrosion inhibitors/accelerators, temperature, ohmic factors, marine organisms, time, and velocity. Although a few of the variables listed were automatically fixed in the experimentation conducted for this study, their importance, in practical applications of corrosion and in particular cathodic protection, cannot be overlooked. They are included here in the interest of such situations.

1. Thermodynamic Feasibility

Thermodynamic theory explains the natural tendency of a reaction to occur on the basis of energy reduction. That is, a reaction between two or more substances will attempt to proceed spontaneously if by doing so, the energy level of the final product(s) is less than the sum of the individual constituent energies prior to the reaction. During such a process, thermodynamic stability is said to have been increased.

This universal principle explains why two metals will react to corrode if they differ in potential and thus determine the probability for a galvanic cell to function. The Nernst equation is based on this thermodynamic reasoning and illustrates that corrosion will not occur unless the spontaneous direction of the reaction indicates metal oxidation [1,9]. Galvanic relationships among various metals in a given environment are commonly listed in corrosion texts and can indicate the direction and relative strength of the corrosion current developed from galvanic coupling.

2. Solid Solution Stability

The effects of alloying can profoundly alter the corrosion behavior of metals. In many cases, the addition of a metal of higher potential to a more anodic metal will yield a solid solution which remains stable when subjected to a particular corrosive environment, exhibiting the characteristics of the more cathodic metal. Uhlig [1] states that regardless of the environment, it is generally necessary to add between 25 and 50 atomic percent of the more noble (less active) component to the solid solution to ensure such corrosion resistance. It is also possible to alloy an active metal with one that tends to passivate under the expected service conditions; here the entire solid solution benefits from the passivation. Ironically, passivity due to unintentional alloying can also be detrimental, as in the case of zinc anodes intended for cathodic protection use. As mentioned previously, trace amounts of iron are expected to produce

dense, adherent, anodic corrosion products leading to ineffective performance.

Unfortunately, alloying can also be detrimental to corrosion performance when only one of the components in the solution is attacked. This leads to selective leaching of the component from the matrix, resulting in a pitted or honeycombed base structure. Common examples of this phenomenon are the dezincification of brass (a copper-zinc alloy) and selective oxidation of chromium from stainless steel alloys at high temperatures.

3. Metallic Structure and Surface Conditions

Microstructurally, a metal is composed of crystal lattice arrays (grains) which nucleate and grow as it cools and solidifies. Since crystal nucleation sites appear throughout the cooling material, a lattice array will grow until it comes in contact with a similar array, forming a grain boundary at the interface. Here a lattice mismatch exists due to different orientations of the contributing arrays and the boundary is a region of higher energy relative to the grains. Grain boundaries are generally anodic regions and also harbor impurities or varying concentrations of alloys in relation to the grain composition [10]. Under certain conditions, intergranular attack can occur where the anodic grain boundary areas are corroded, loosening grains and greatly reducing a material's strength.

Corrosive attack of a metallic surface can also be affected by the presence of inclusions and other nonuniformities. Inclusions, which are random, microscopic regions of

impurities, can be more or less active than the surrounding metal and thus form microanodes or microcathodes. Microanodic inclusions obviously tend to be shortlived but microcathodic regions can have a substantial affect on the adjacent anodic matrix. Relatively high current density in the vicinity of such areas can lead to dense corrosion product deposits or the formation of large pits. Nonuniformities such as scratches on a finely ground surface can also be relatively anodic [8]. Careful polishing tends to decrease initial surface corrosion but its benefits are at best temporary in a caustic medium.

4. Mechanical Factors

In many situations, stress, strain, and mechanically abrasive actions will modify the corrosion characteristics of a metal. In effect, they can impart additional energy to the metal and thus lower thermodynamic stability or cause a breach in the continuity of a passive and protective film [8]. Coldworking is a common example where substantial energy can remain in the metallic lattice causing numerous dislocations along grain boundaries, inviting corrosive attack. Passive film disturbance from abrasion is possible but can also result from the application of stress since the film ductility generally differs from that of the metal. Finally, the conjoint action of stress and corrosion can promote accelerated cracking since obstructions to such cracks are demolished by corrosive action. Similarly, evidence of increased corrosion at crack tips in the absence of obstructions exists. Several hypotheses currently exist which attempt to

explain this phenomenon. Regardless of the mechanism, mechanical factors constitute a complex interplay of metal, interface, and environmental properties on corrosion behavior [9].

5. Electrolyte pH.

A broad range of solution pH values can have a two-fold influence on corrosion behavior. It can directly affect the hydrogen ion concentration's influence on an electrode process or indirectly, influence a change in the solubility of the corrosion products and thus enhance the possibility of changes in protective film formation [8]. Fortunately in the marine environment, values of pH remain relatively constant among geographic regions with average values of 8.0 to 8.3 near the seawater surface [11]. Similar to ocean conditions, synthetic seawater pH values were kept within the above range during experimentation.

6. Salt Concentration

Generally the solubility of oxygen in a solution decreases with increasing salt concentration but such variations are small in the ocean environment. Monney states that corrosion rates due to differences in salt concentrations, which average between 33 and 35 parts per thousand in the open ocean, will not fluctuate more than 10% to 15% [11]. This factor was kept constant during laboratory studies and thus oxygen content also remained invariant at room temperature.

7. Corrosion Inhibitors/Accelerators

Under certain conditions, the addition of small amounts of substances to the electrolyte can subtantially alter corrosion behavior and in most cases such additions are used to

inhibit corrosive attack. Inhibitors may affect the anodic, cathodic, or passivating tendencies of a material [8]. Considering anodic inhibitors, primary concern is to eliminate the oxidizing action at the electrode. If it is desirable to produce an anodic-isolating film, care must be taken to cover the entire region to avoid extremely localized pitting. Deaerating inhibitors serve to reduce cathodic processes or alternatively, a cathodic-isolating film can be formed.

Inhibitors may also be classified as absorption types, hydrogen evolution poisons, or scavengers [9]. With the first method, the inhibiting substance is absorbed on to the surface of the metal where it reduces dissolution and reduction processes. Hydrogen evolution poisons work well in acidic solutions but become ineffective under conditions where cathodic reactions are controlled by other processes such as oxygen reduction. Finally, scavengers inhibit attack by removing corrosive reagents from electrolyte solutions. An example is solution deaeration. Corrosion accelerators perform in an opposite fashion to inhibitors.

8. Temperature

The rate of electrochemical corrosion usually increases with increasing temperature and most frequently the relationship is logarithmic as expressed by the Arrhenius equation:

$$U = A \cdot \exp^{-(Q/RT)}$$

where U is the speed at which corrosion progresses and T is

the absolute temperature [8]. (A, Q, and R are constants for a given situation; exp is the base of natural logarithms.)

It has been reported that the conductivity of seawater nearly doubles as the temperature increases from 0° to 25°C and that corrosion rate in this environment should double with an increase in temperature of 10°C [11]. Uhlig states that for every 30°C rise in temperature, corrosion rates generally double when they are controlled by the diffusion of oxygen [1]. Above 80°C, this relationship does not continue since the solubility of oxygen decreases with increasing temperature [8].

Although shipboard zinc anodes typically operate in a temperature range between 0° and 30°C, no attempt was made in the present study to investigate the effects of this variable on their performance.

9. Ohmic Factors

The electrical resistance of a galvanic cell primarily exists in the current path through the electrolyte. Factors to be considered in any arrangement of this type include the specific resistivity of the electrolyte, the ratio of anodic-to-cathodic areas, and the geometric configuration and position of such regions [8]. These factors, as applied to the experimental apparatus used in this work, are accounted for in another section of this report.

10. Marine Organisms

Microscopic organisms are common to the ocean environment and are usually detrimental considering their effects on corrosion. Adherent colonies of the organisms

can be found on most ocean structures. As they grow and cover (foul) various metallic surfaces, discontinuities in their covering can result in localized corrosion of the remaining bare metal. In addition, the composition of the electrolyte near the organisms may be altered due to their biological processes.

Another problem resulting from the fouling is the creation of an oxygen concentration cell. Here the covered metal surface is depleted of oxygen and thus becomes anodic to surfaces still in direct contact with the electrolyte. Fortunately, such organisms do not affect anodic zinc corrosion due to the high rate of removal of the deteriorating surface. The use of synthetic seawater in the laboratory eliminates their presence entirely.

11. Time

The amount of corrosion in any situation is time dependent. Serious efforts were undertaken to rigidly control the amount of exposure time of each specimen to the corrosive environment during experimentation. Procedural specifics are contained in Section II.

12. Velocity

There is a complex dependence between corrosion rate and solution/electrode velocity. In most cases, velocity effects will increase the rate of attack by supplying more oxygen to cathodic areas or acting to erode passivating anodic films. Also, if cathodic processes are governed by concentration polarization, velocity will eliminate the concentration and increase the corrosion rate [9]. Exceptions

to these instances include crevice corrosion and pitting, where velocity effects remove deleterious chloride ions and supply the oxygen necessary to form a passive film. Depositions of silt or other particles, which can result in destructive oxygen concentration cells, are also disturbed by the velocity factor [9]. Corrosion inhibitors are better supplied to metal surfaces when non-stagnant conditions prevail.

The effect of velocity on zinc anodes used for cathodic protection purposes is thought to be beneficial to their performance in that anodic corrosion products are constantly removed, exposing bare metal for galvanic attack. Problems encountered with zinc sacrificial anode passivation on inactive reserve vessels support these convictions.

C. FURTHER ANODIC ZINC CORROSION RESEARCH

As mentioned, one of the earliest contributions to the development of zinc alloys for galvanic anodes was the discovery of the deleterious effects of substantial iron content by several investigators. More recently, various additions to the literature have been made which warrant consideration. For example, results of the introduction of small quantities of several elements, singly and in various combinations, into high purity zinc have been reported. Subsequently, some explanations for these alloying effects, based on microstructural observation, have been offered. Recently, work at the Naval Postgraduate School has sought to examine and characterize anodic zinc corrosion product morphology, primarily via scanning electron microscopy techniques. From such

investigations, a dissolution-precipitation process and microstructural corrosion model have been postulated. Salient conclusions follow which have been drawn from this research of the past two decades.

Aside from their recommendation of a 0.0015% limit of iron in commercially pure zinc, Teel and Anderson, in 1955, were among the first to report that the addition of aluminum increased the current output of the anodes [12]. It appeared as though this alloying cancelled the effects of iron; they found that 0.11% of it in zinc which contained as much as 0.033% iron provided as much output as unalloyed zinc that met iron content specifications. These alloying effects were carried further by Reichard and Lennox in 1957, who discovered that even greater anode performance and iron tolerance was realized with simultaneous additions of aluminum and cadmium of 0.1% and 0.05% respectively [13]. The new alloy was not greatly affected by varying current densities or electrolyte temperatures. Corrosion products were substantially less adherent and thus countered passivation tendencies. The team also conducted experiments with high purity zinc concluding that its optimum iron content was on the order of 0.0002% but still found this result inferior to the double-alloy anodes. In 1960, Carson added supporting evidence concerning these realizations [14].

In a laboratory evaluation of zinc anodes in seawater, Carson, Phillips, and Wellington sought to control anode current density while attempting to shed more light on the consequences of alloying [15]. Previously, corrosion experiments

were subject mostly to the natural emf of the test cells. Realizing that anode passivity was due to a corrosion product film, they chose to measure the potential of anodes of varying compositions at selected current densities in order to determine which composition was least polarized with time over a span of current densities. Using pure zinc anodes, the group found no optimum level of iron concentration and noted that at constant current density, the specimens tended to polarize with time, the degree of polarization increasing with iron content. At high current densities, a marked change in corrosion behavior occurred as iron content increased from 0.001% to 0.002%. Using zinc anodes with varying amounts of aluminum, there appeared to be an optimum aluminum content between 0.3% and 0.6% aluminum and the presence of this metal improved anode performances significantly. More interesting was the fact that given the optimum level of aluminum, there corresponded an optimum iron content between 0.001% and 0.005% so that anodic polarization was minimal. Finally, comparing two ternary alloys (0.1% aluminum plus 0.05% cadmium and 0.5% aluminum plus 0.07% silicon) to a zinc alloy containing an optimum amount of aluminum, they found little difference among corrosion behaviors.

Somewhat conflicting information to the above conclusions was derived from the research efforts of Waldron and Peterson whose experimental apparatus provided no control of anodic current density [16]. Their convictions were fairly

analogous to earlier reports suggesting that aluminum and cadmium must be simultaneously present for best possible results. They also showed that the benefits derived from cadmium increased up to a 0.02% cadmium concentration but then do not vary substantially with further additions. Similarly, concentrations of aluminum greater than 0.5% were not found to be significantly advantageous. Minimum amounts of aluminum and cadmium were set at 0.1% and 0.25% respectively. Providing these restrictions were upheld, iron content of up to 0.006% in zinc was said to be tolerated.

Military Specification A-18001H, written for corrosion preventive anodes used aboard ships, appears to have accepted the predictions of the various studies referenced above. Compositional requirements for alloyed zinc are explicitly stated in this specification, with the ultimate intent of obtaining anodes whose adherent corrosion products remain soft and/or maintain a high degree of porosity. The specification requirements are listed in Table II.

In 1964, R. T. Southin's unique examination of anode microstructures resulting from common alloying additions attempted to explain why the alloys affected anode performance as they did [17]. Interest concerned the solid solubilities of the alloy trace constitutents and also their ability to form compounds with any iron present. Although both aluminum and cadmium tended to refine the microstructural grains, Southin contended that such changes would not alter corrosion performance.

Iron's low solid solubility in zinc leads to the formation of an iron-zinc compound when iron content is greater than 0.001%. The compound is 6% iron. Because investigations have shown that anodic behavior is affected even at iron levels below 0.001%, Southin justifiably suggests that both the iron-zinc compound and the iron still in solution affect the corrosion product formed.

Due to the low solid solubility of aluminum in zinc (0.3% aluminum), and the very low solid solubility of silicon in zinc, these two elements also form compounds in the anode but with the available iron as Fe_2Al_5 and FeSi respectively. Corrosion resistant, these compounds eliminate iron in the metallic matrix, but do not contribute to corrosion products formed. Since aluminum levels can be lower than 0.3%, yet continue to enhance anode corrosion character, Southin suggests that the effects of aluminum in solid solution must also bear significance, probably in the type of corrosion product formed as was the case with iron in solid solution. Subsequent to FeSi formation, iron levels were below 5 ppm.

In zinc alloys containing aluminum, silicon, and iron, FeSi was formed preferentially to Fe_2Al_5 or an iron-zinc compound. It should be pointed out though that because of its nil solubility in zinc, additions of silicon to zinc must be introduced in the form of an aluminum-silicon alloy to be effective. Thus it may be difficult to eliminate large amounts of iron with silicon alone.

An addition of 0.05% cadmium went immediately into solid solution forming no compounds. Apparently it is beneficial

to anode corrosion in this state. Also, cadmium was not observed to affect Fe_2Al_5 formation when both elements were added to zinc simultaneously.

From the above work, Southin logically concludes that two mechanisms exist by which alloying additions can concurrently affect anodic zinc corrosion:

1. Elemental additions could cause the formation of compounds which reduce the detrimental concentration of iron, e.g., Fe_2Al_5 and/or FeSi.

2. Elemental additions which have some solid solubility in zinc could alter the characteristics and/or composition of the corrosion product, yielding a less adherent and/or more porous film.

From another viewpoint, Gliszewski and Malinowski have more recently collected statistical data, from studying the microstructures of shipboard zinc anode specimens, which denotes that such microstructure may be a factor in this type of corrosion [18].

Research throughout the 1950's and 1960's resulted in some significant improvements in zinc anode performance but despite serious efforts, a totally dependable zinc anode for cathodic protection needs was not developed. Shipyard cathodic protection engineers have continued to find some passivated galvanic zinc alloy anodes even when the alloys adhered to compositional specifications. This performance uncertainty has led to varying usage of this sacrificial method in the fleet and points to the increased popularity

and choice of impressed current cathodic protection systems on major combatant vessels in recent years.

In 1973, Bornholdt and Perkins inaugurated scanning electron microscope examinations, of the growth of anodic zinc alloy corrosion product films, as a unique alternative approach to the passivation problem [19]. They discovered that the films were composed of dense but microscopically porous arrays of anodically electrocrystallized hexagonal zinc oxide (ZnO) plates. Following a one week zinc-to-steel galvanic coupling in natural seawater, approximately 10^6 ZnO platelets per square centimeter of anode surface were present. Average-sized platelets were typically 30 μm in diameter and several μm thick, and formed with ZnO crystal basal planes parallel to the broad, slow growth platelet faces. The plates were located close to perpendicular to the zinc alloy surface.

Todd and Perkins continued microscale investigations of anodic zinc corrosion products in 1974, concentrating primarily on the nucleation and growth process of the passivating film in natural and synthetic seawater solutions [20,21,22]. Several significant conclusions resulted from these studies which may ultimately lead to solution of this persistent problem. Zinc specimens, conforming closely to Mil Spec A-18001H [5], were corroded by individual attachment to a steel plate and submersion of each assembly in a beaker of saltwater solution. Microscopic examination of anodic surfaces, following controlled times of exposure to galvanic

attack, revealed that ZnO platelet nucleation occurs on these surfaces in approximately 10 minutes. It was postulated that a thin, supersaturated layer of dissolved zinc ions above the metal surface made such nucleation possible, but whether platelets initially materialized on the metal or within the ion layer, prior to settling on the surface, was not confirmed. Platelets originated near microcathodic surface asperities and inclusions where the corrosion current density, and thus dissolution rate of metal ions, was initially highest. The base alloy inclusions were also suspect as sites of initial passivating film formation subsequent to long term galvanic exposure and are considered in the development of the team's microstructural corrosion model. Here it is proposed that the local field lines, altered by these microcathodic surface irregularities, cause zinc oxide platelets to settle and grow parallel to the anode surface. Also, x-ray diffraction patterns and energy dispersive x-ray analysis were used to aid identification of secondary corrosion products. Among other compounds, zinc carbonate ($ZnCO_3$) and a zinc chloride-based ($ZnCl_2$) complex appeared to be evident.

Todd proposed that the mixed-potential polyelectrode concept provided an acceptable vehicle with which to explain the metal dissolution phenomenon [22]. According to this concept, several independent electrode reactions are possible on the surface of a corroding metal and are related by a difference in potential existing between the metal and the

electrolyte. This potential difference in turn governs the direction and magnitude of electrical current flow at the metal/solution interface. Further theoretical implications discount the necessity of fixed anodic and cathodic metallic regions, allowing instantaneous shifts in current over the surface. Further discussion of this concept will be postponed until specifically needed.

As mentioned, this study continues to examine anodic zinc corrosion products via scanning electron microscopy but concentrates on the effects of anode velocity and current density on product formations. Knowledge gained from the undertaking should be of a practical and scientific nature and provide more insight to future investigators concerned with eliminating anodic passivation tendencies.

II. EXPERIMENTAL PROCESS

A. APPARATUS

Studies of effects of anode velocity and current density on corrosion are compatible to the extent that it was possible to design a single experimental device, capable of exposing zinc specimens to these variables separately or simultaneously. Figure 1 depicts the experimental set-up which included: a cylindrical tank container, rotating disk assembly, current generator/power source, and a digital voltmeter and frequency counter as monitoring instruments.

1. Tank Assembly

The exposure tank, which contained the synthetic seawater electrolyte, was constructed entirely of plexiglass. The vessel was 18 inches (45.72 cm) in diameter and filled to a level of approximately 11½ inches (29.21 cm) to hold 12.7 gallons (47.95 l). A system of plexiglass baffle strips was installed symmetrically along its interior and bottom in order to keep the electrolyte as stationary as possible during traveling electrode experiments. The relatively motionless fluid/traveling electrode situation created by this arrangement was somewhat analogous to that encountered by shipboard zincs. The tank bottom was also fitted with an embedded, 14 inch (35.56 cm) diameter aeration canal which allowed compressed air to be bubbled through the liquid from an array of 12 air holes spaced 30° apart. A regulator

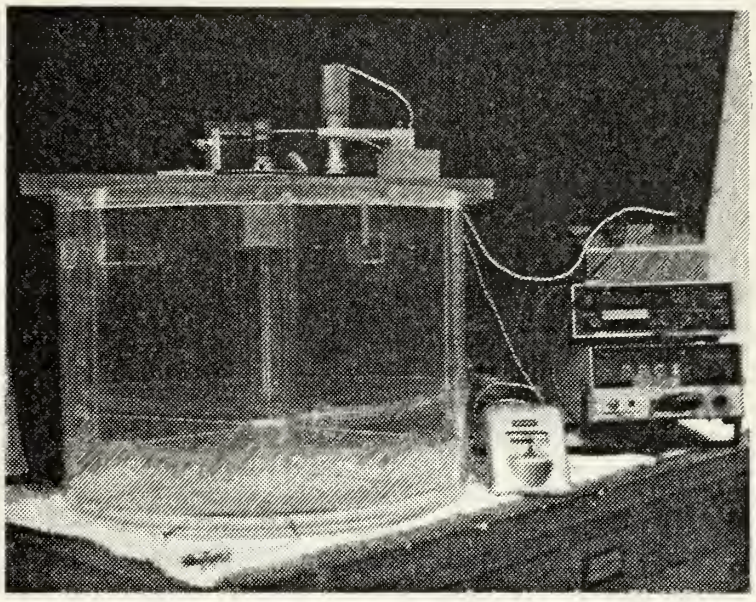

Figure 1

Experimental apparatus showing exposure tank, rotating disk assembly, timer, current generator, digital counter, and digital voltmeter

attached to the air supply provided precise control of air flow to ensure that the electrolyte was saturated with oxygen. The bubbling also provided a vertical circulation pattern to eliminate potential concentrations of corrosion products in the solution during tests. Figure 2 exhibits the exposure tank construction.

A rotating disk assembly was used to expose zinc samples to velocity effects. It consisted of a 12 inch (30.48 cm) diameter, ½ inch (1.27 cm) thick plexiglass disk suspended 8 inches (20.32 cm) below electrolyte surface by a 1 inch (2.54 cm) diameter plexiglass shaft. The shaft was connected via a pulley arrangement to an electric motor. Variations in pulley size allowed disk speed to be controlled from 6 to 210 rpm. Figure 3 illustrates the assembly.

Each zinc sample was located in the disk underside in a small rectangular slot near the disk perimeter as shown in Figure 4. Distance from the center of the disk to the center of each sample was 5.70 inches (14.48 cm). The slot was machined to accommodate the 7/16 in x 7/16 in x 3/16 in (1.11 cm x 1.11 cm x 0.48 cm) specimens with minimum tolerance so that once in place, they were flush with the disk surface; clearance between the sides of the zinc sample and the plexiglass slot was also minimized. A modicum of solution disturbance was realized with this scheme.

Figure 5 is a detailed drawing of the specimen slot. As is shown, samples were held in place with a plastic setscrew which was threaded into a tapped hole in each of them.

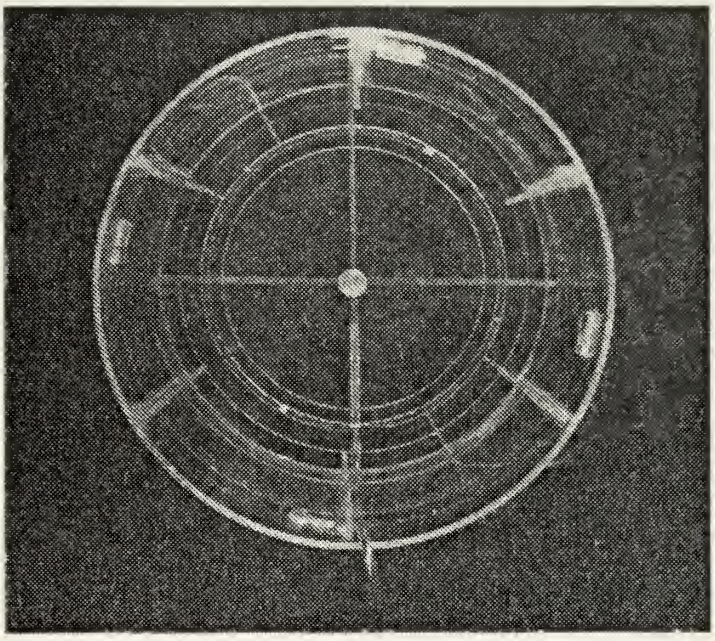

Figure 2

Exposure tank construction

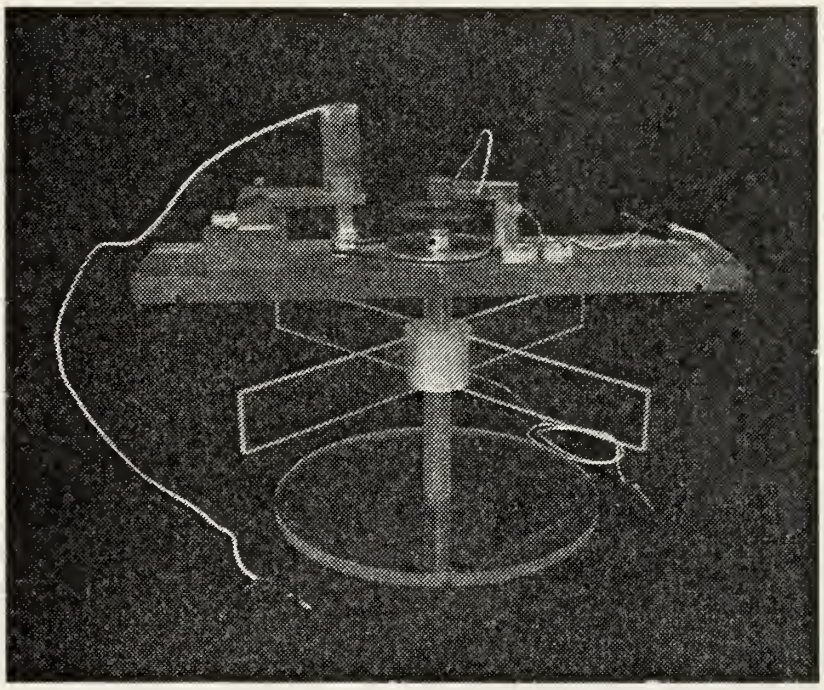

Figure 3

Rotating disk assembly

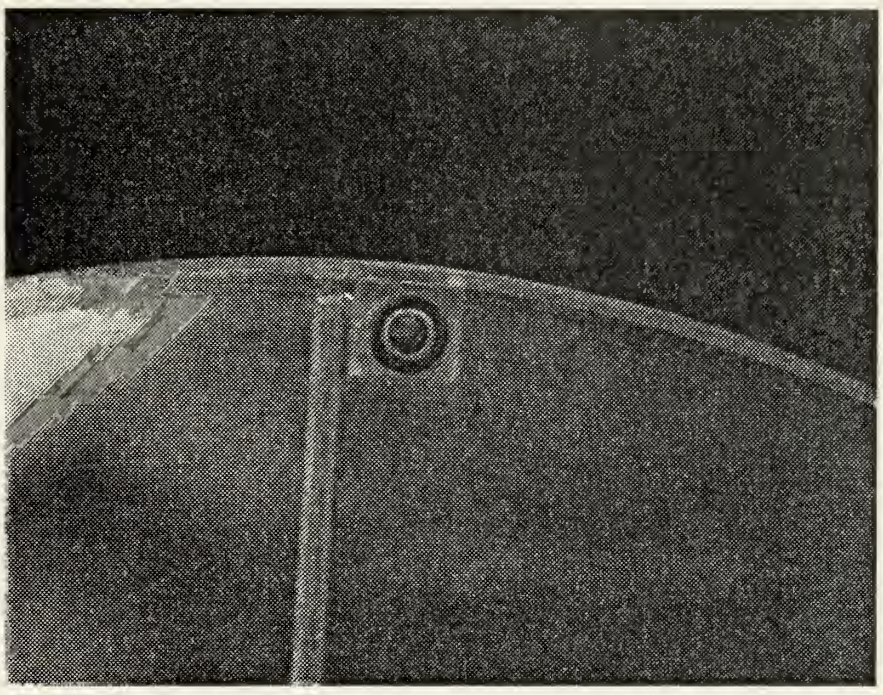

Figure 4

Zinc specimen slot in the rotating disk

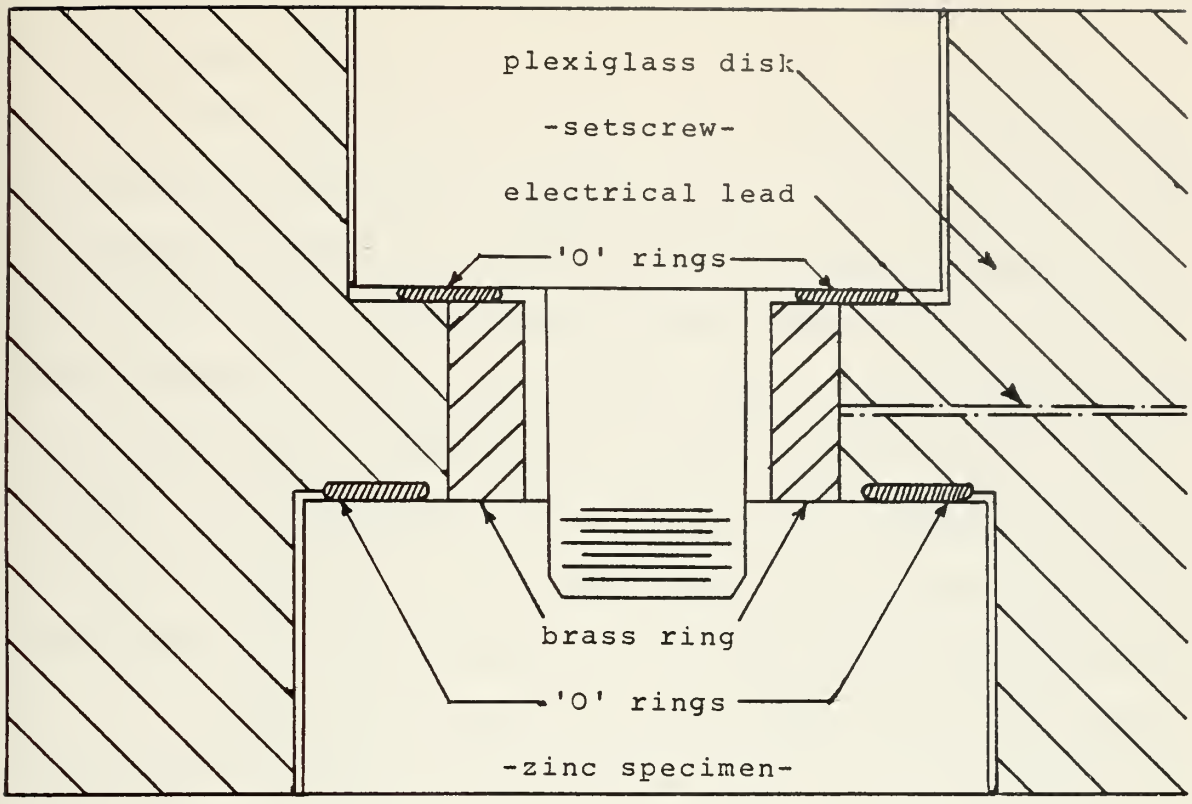

(8 times actual size)

Figure 5

Detailed drawing of the specimen slot showing watertight electrical lead, brass ring electrical contact, and rubber 'O' rings

The screw entered the disk from its top surface and when in place, the top of its head was flush with the surface.

The anodic zinc current was controlled using an impressed galvanostatic current system. Figure 5 reveals that electrical contact was accomplished by using a brass ring to form the inner wall of the setscrew hole in the disk. As the specimen was secured into the slot, it was forced against the brass ring to complete this part of the circuit. Two rubber 'O' rings were used to isolate the brass/zinc connection from the electrolyte, one under the setscrew head and one around the outer perimeter of the brass/zinc interface.

Current was supplied to the brass ring by a copper wire placed within a hole drilled along the disk radius to its center. At this point the wire passed into the hollow interior of the connecting drive shaft and then up out of the tank. In this way current was delivered to the zinc via a watertight route to guarantee that only the specimen would corrode. The connection was suitable under stagnant or rotating conditions.

As pictured in Figure 3, four plexiglass baffle blades were fastened at 90° intervals to a hollow plexiglass tube through which the shaft passed. The blade tips fit into retaining grooves along the sides of the tank, slightly beneath the level of the fluid. Besides helping to keep electrolyte disturbance minimal, this upper baffle structure acted as a loose collar bearing against shaft wobble.

Above the baffles, the shaft passed through a plexiglass board which supported the entire spinning assembly. Inert teflon bearings coupled the shaft to the board which rested on top of the tank walls. The underside of the board had ¼ inch (0.64 cm) deep grooves cut to the curvature of the tank sides so that the assembly remained centered over the receptacle during operation.

The top of the shaft was fitted with a pulley wheel, a 60-tooth gear, and a brass ring. A magnetic pickup, positioned near the gear and attached to the digital frequency counter, sensed a magnetic flux as each tooth passed during shaft rotation. These flux signals were instantaneously converted into rpm and displayed by the counter. A copper brush was positioned to rest against the brass ring, to which was soldered the copper wire from the interior of the shaft. Connection from the current source to the brush allowed the current of the zinc anode to be controlled regardless of its velocity.

Platinum was chosen as the impressed current cathode because of its non-fouling characteristics regarding the electrolyte. When held at potentials higher than other metals, only hydrogen bubbles are released which float to the surface of the liquid and escape. This second electrode assembly consisted of a thin, 1.50 inch (3.81 cm) diameter platinum disk and is shown in Figure 6. It was positioned to rest on top of the bottom baffles and at the center of the tank, approximately 1.25 inches (3.18 cm) below the plexiglass disk.

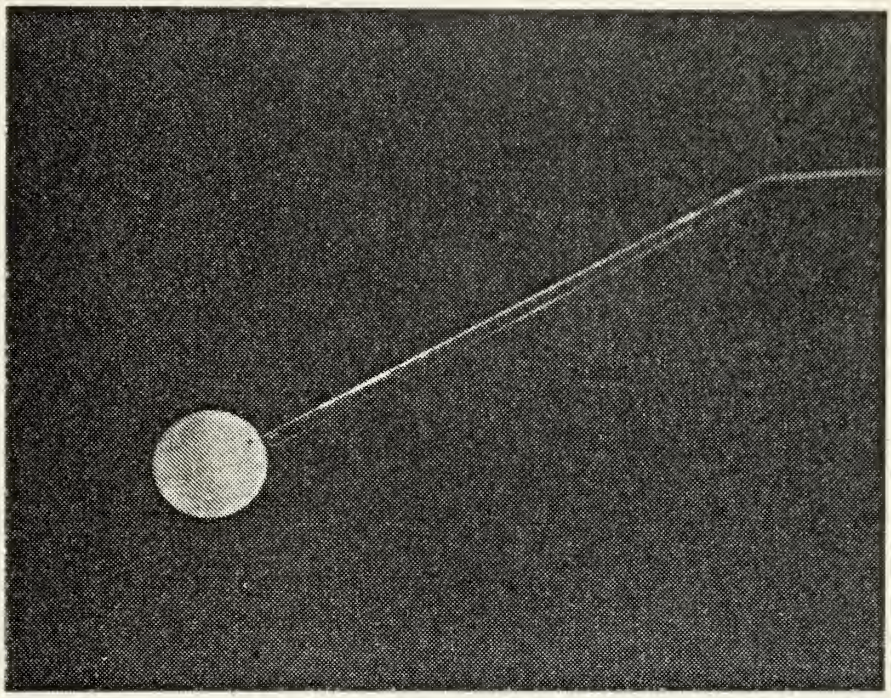

Figure 6

Platinum disk impressed current cathode
showing watertight electrical connection

Thus as the entire apparatus was operated, in either the spinning or stationary mode, the distance from the center of the cathodic disk to the center of the anodic zinc was always constant and equalled 5.84 inches (14.82 cm).

As with the zinc electrode, construction was designed to ensure that the platinum disk remained the only cathode in the tank during experimentation. It was arc welded to the tip of a platinum wire which passed immediately into a sealed piece of glass tubing. Within the tube, the wire was electrically connected to the current source lead by their mutual immersion in liquid mercury. The source lead passed from the glass tube through sealed plastic tubing and out of the tank so that the platinum disk was ultimately connected to the current source via a watertight route. The tubing was secured to the bottom baffles and sides of the tank with inert fasteners, to avoid entanglement during disk rotation.

2. Current Generator and Voltage Source

To accomplish the objectives of this work through experimentation warranted the design (by Mr. Tom Christian of the Department of Mechanical Engineering) of a multi-mode power source whose wiring schematic appears in Figure 7. A written description of this device by Mr. Christian is attached as Appendix B. The device was capable of supplying current necessary for corrosion study as well as that required by the motor to rotate the plexiglass disk. Equipped with two separate circuits, (a voltage and current generator) it could perform both functions simultaneously or singly.

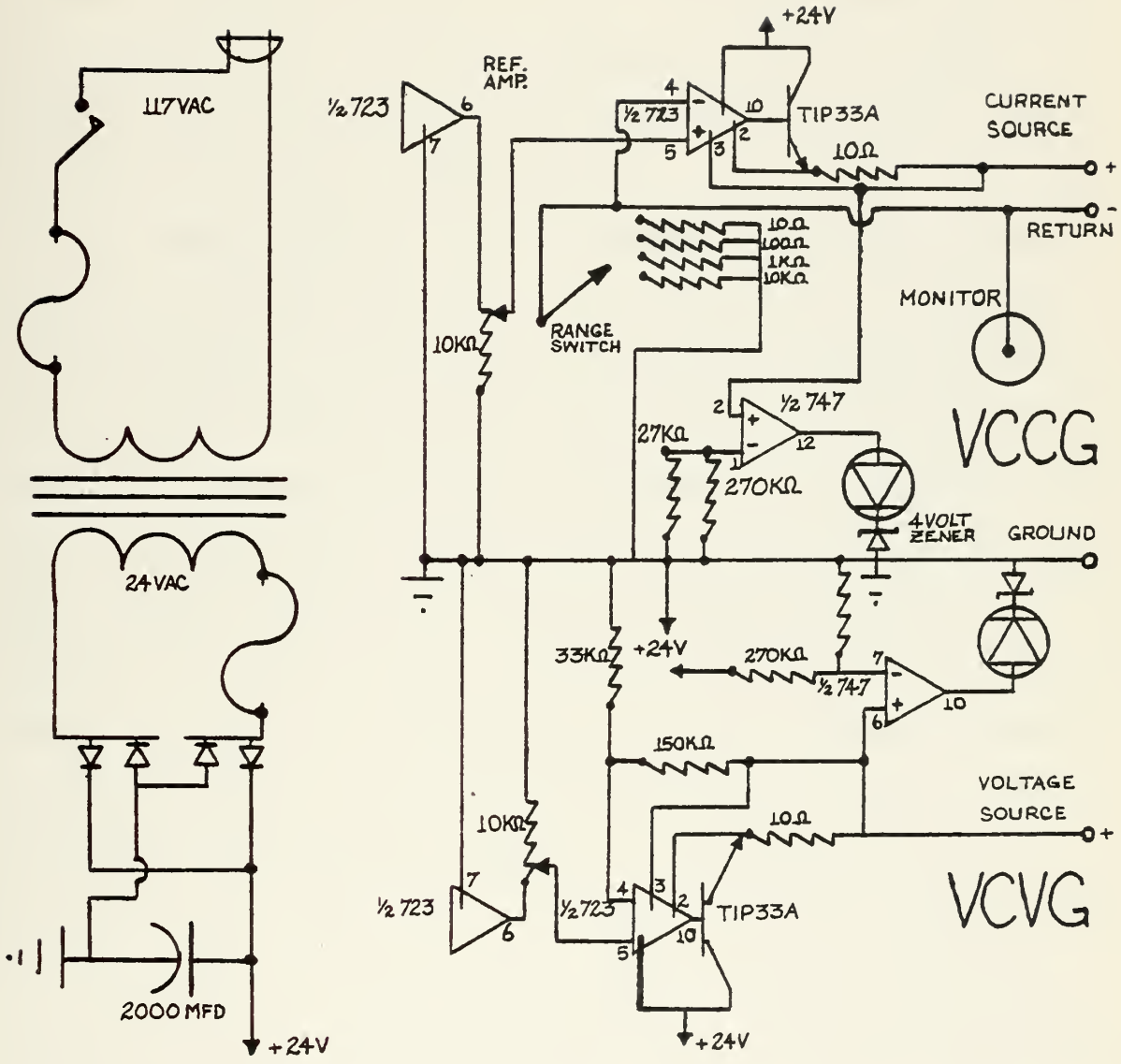

Figure 7

Schematic of Voltage Controlled Current Generator and Voltage Controlled Voltage Generator [App. B]

The voltage-controlled voltage generator was a fairly simple power supply consisting of a positive voltage regulator with an outboard pass transistor and current limiting network providing a regulated D.C. voltage of approximately +1.5 volts to +30.0 volts at currents of up to 1 ampere [App. B]. A potentiometer made it possible to control this current and thus the disk motor rpm.

Current output from the voltage-controlled current generator to a zinc specimen was governed by the selection of a particular voltage across one of four precision resistors and this voltage was monitored with the digital voltmeter. The chosen resistor was automatically placed in series with the load (anode/cathode set up) so that the current through the load was identical to that through the resistor (Kirchoff's Law). Circuitry logic provided the current necessary to maintain the selected voltage. Dividing this voltage by the value of resistance chosen yielded the current through the specimen. The precision resistor values were 10, 100, 1000, and 10000 ohms which greatly simplified converting monitored voltage to circuit current. Maximum current available was 0.75 amps (7.50 volts with the 10 ohm resistor).

The dynamic response of this configuration was on the order of 15 microseconds and overall regulation was 0.1% of full scale of the selected range [App. B]. It was possible to control specimen current to $\pm$ 2 microamps regardless of anode velocity.

Light emitting diodes served as overload indicators for both the current and voltage generators, and thus signalled the operator that the potentiometer controlled range was inadequate. These glowed at excessive motor rpm or when the circuitry was unable to supply the current necessary to deliver a selected voltage across a precision resistor. Due to the small surface area of the zinc samples, current densities required during experiments never exceeded the capacity of the equipment.

3. Scanning Electron Microscope and X-ray Analyzer

After exposure to the corrosive environment, the surface of each zinc sample was studied with an S4-10 Stereoscan Scanning Electron Microscope (SEM), shown in Figure 8. Use of this device enabled accurate characterization of the effects of experimental variables on corrosion product morphology. Analytical work of this nature in the field of corrosion research has only recently become a reality and at present, its future possibilities seem unbounded.

Concerning the examination of corrosion films in this study, the capabilities of the SEM when compared to conventional light microscopy are impressive. Due to limited depth of focus, the latter method of investigation requires that a specimen be mounted, ground, and polished prior to observation. The technique is time consuming and requires substantial expertise to ensure reliable satisfactory results. The SEM depth of focus is at least 300 times greater at equivalent magnifications such as employed in this study, so that

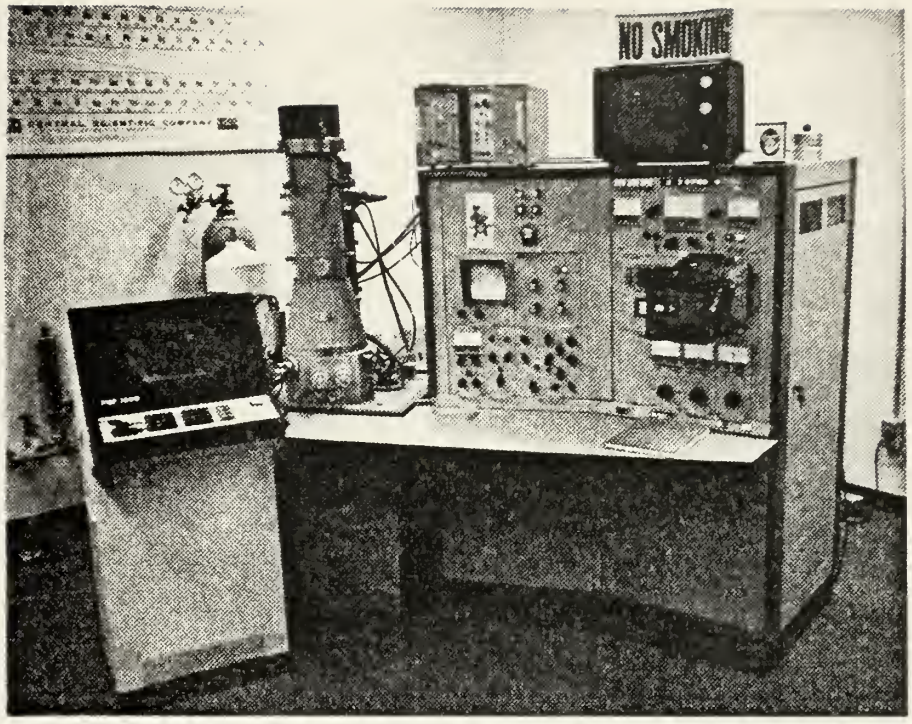

Figure 8

Cambridge Model S4-10 scanning electron microscope (SEM) and Princeton-Gamma-Tech PGT-1000 X-ray Analyzer

excellent resolution of the material may be obtained without prior presentation. In addition, a useful magnification range of up to 20,000X is possible, an increase of about 20 times over optical instruments. The apparatus provides the operator with the ability to translate the specimen in the x, y, and z directions, to rotate it clockwise or counter-clockwise a full 360°, and to view it at angles of incidence from approximately 0° to 90°. Specimens of up to ½ inch (1.27 cm) diameter and about ½ inch (0.64 cm) thickness may be examined.

Basically, the internal operation of the SEM is similar to a conventional microscope except that it manages beams of electrons in a vacuum with magnetic lenses rather than light waves with optical lenses as in the latter case. A fine beam of electrons is emitted from a tungsten filament and accelerated to approximately 20 kV. Electromagnetic lenses focus the beam which is scanned over an area of 0.04 in^2 (0.25 cm^2) or less on the sample surface, depending on magnification. Bombardment of this surface by electrons results in its emission of secondary electrons which are collected by the SEM to produce the desired image. This is accomplished by focusing the secondary particles onto a scintillation device which, by definition, contains a crystal that emits light when struck by ionizing radiation. The device is coupled to a photomultiplier and several amplifiers which ultimately deliver the signals to the cathode ray tube modulator. The cathode ray visual presentation, due to

modulator stimulation, is synchronized with the electron beam scan. Because the secondary electrons collected have been emitted at various angles from various locations, the picture developed is three-dimensional in appearance and its quality differs little from that of the actual specimen surface. Light and dark areas in the display correspond to variations in the amount of secondary electron signal from place to place on the specimen, and therefore, a contrast very much related to topographical variations results. Contrast can also arise due to varying degrees of conductivity on the specimen surface; where more conductive, fewer secondary electron emissions occur which directly affects the signal reaching the modulator. Being able to discern differing degrees of conductivity on the specimen surface is very usefully applied to image analysis of corrosion products in corrosion research.

Bombardment of the specimen by the SEM electron beam also causes it to emit x-rays which are valuable in elemental analysis of corrosion products. Coupled to the Naval Postgraduate School SEM is a Princeton Gamma Tech 1000 energy-dispersive x-ray analyzer, Figure 8, which made this second type of investigation possible.

X-rays in general are fluoresced at various energies, each x-ray corresponding to a particular element. Thus there can be direct identification of elements present from the energies fluoresced. A solid state Si(Li) semiconductor detector within the SEM specimen chamber receives these multi-energy rays, converts them into electrical signals, and sends

them to the analyzer. Consequently, after selective processing, an energy spectrum of signals is displayed. Since each horizontal increment of the spectrum relates to a certain energy level, spectrum peaks that appear imply relatively large amounts of specific x-ray energies emitted and thus their matching elements which comprise the specimen. Because numerous trace elements are found in ship hull zinc, the analyzer can be used to determine if their presence affects the corrosion process, its rate of progress, or corrosion product morphology.

B. PROCEDURE

Zinc samples used in experimentation were cut from a 22-pound (48.51 kg) zinc alloy slab which was intended for cathodic protection use as a ship hull anode. Spectrographic analysis revealed that the alloy was 99.99% zinc with trace elements of lead, iron, cadmium, aluminum, copper, and silicon (see Table I). This composition corresponds closely with Military Specification A-18001H for ship hull zincs [5].

Prior to exposure, the surface of each specimen underwent a standard preparation sequence, so that the effects of varying surface topography, resulting from the rough machining process, would be minimized and the reproducibility of data improved. Each sample was ground with 600-grit paper, gently rinsed with tap water and alcohol, then dried with a jet of freon gas. Figure 9 shows a typical metal surface, ready to be used in an experiment, at magnification 3000X.

All experiments were performed with a laboratory-prepared electrolyte solution of synthetic seawater. Appendix A

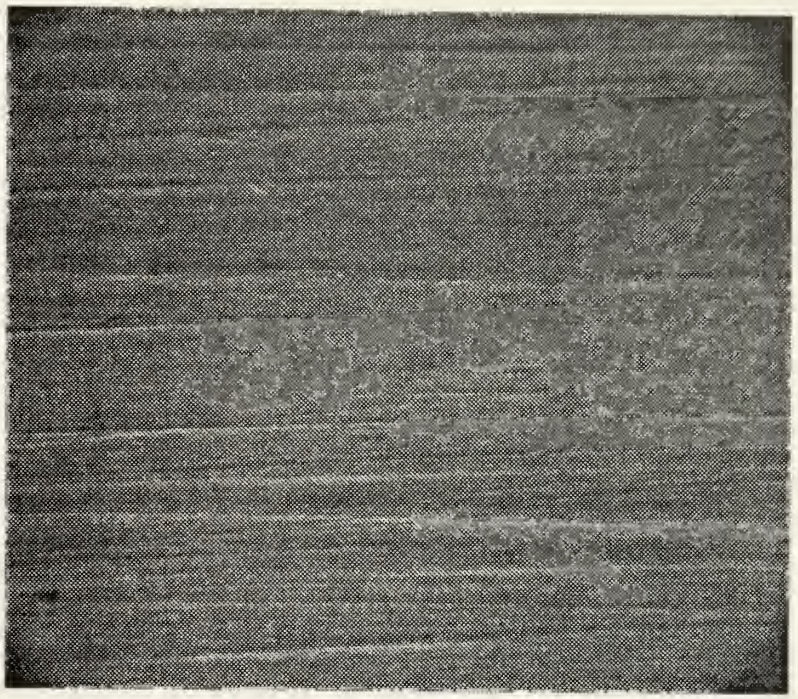

Figure 9

Scanning electron microphotograph of
initial polished zinc surface, 3000X

contains the specification standards followed and chemicals used in its preparation. Due to the large capacity of the exposure tank, it was easier to produce and handle a smaller quantity of concentrated solution which could be properly diluted once inside the tank. Synthetic seawater specifications required that its pH values range from 8.0 to 8.4 with conductivity measurements between 39.0 and 45.0 millimhos [23]. Before each set of experiments, the solution was tested and adjusted if necessary to meet these restrictions. Usually only a small addition of distilled water, to compensate for evaporation losses, was needed to bring seawater quality to within proper limits.

Once a specimen was fastened into the rotating disk slot, but before being lowered into the electrolyte, several checks were made to ensure that the corrosion current delivered would be that actually prescribed by the experimental plan. The digital voltmeter contained a built-in reference for its calibration and its accuracy was repeatedly verified. When the calibrated voltmeter was attached to monitor the current generator, it was possible to read what output the generator was adjusted for by connecting a 1000 ohm resistor between its terminals. The resistor acted as the load in place of the corrosion circuit, thus allowing the generator's potentiometer dial to be approximately preset for the specified experimental current value. This practice eliminated the chance of a corrosion current surge when the actual circuit was completed. Finally, the specimen's electrical contact with

the brass ring inside the slot was checked by temporarily connecting the rotating assembly's circuit to the current generator. This was accomplished, while still outside the tank, by joining one generator lead to the copper brush and then holding the second lead against an edge of the specimen just long enough for response from the digital voltmeter.

Due to a very limited treatment of this research topic in the literature, a strict experimental plan was not developed until some preliminary investigations with the apparatus were undertaken. Before variations in anode velocity could be studied, a suitable constant current-time product had to be chosen. It was reasoned that a current-time product great enough to produce the characteristic, hexagonal zinc oxide platelet corrosion products, formed during recent experiments by Todd, would suffice as a starting point [22]. Except in a few cases, Todd's zinc specimens underwent galvanic attack resulting from a simple zinc-to-steel couple with a cathode-to-anode area ratio of approximately 50:1, and the anodic current was not measured. Zinc corrosion in the present study was entirely produced and controlled by the current generator designed and it was possible that such a system would not create the same electrical environment as experienced by shipboard galvanic zinc anodes. To prevent such occurrences, the current flow of a galvanic cell identical in most respects to Todd's setup was first measured. A current density of approximately 10mA/in^2 (1.55 mA/cm^2) of zinc surface was determined and found to produce corrosion

tendencies and products identical to Todd's, when environmental conditions in both studies coincided. Observations also indicated that the effects of microcathodic sites, of significance in the previously cited work, were unaltered by this approach. Corrosion times long enough to form dense, coherent, passivating films as in the prior study, were not examined in the present study, so that effects due to impressed current at this stage of film development were not encountered.

It follows from the introductory discussion on cathodic protection and corrosion that a metal surface will undergo some corrosive activity the instant it is immersed in an electrolytic solution. The principle considerations here pertain to the existence of microanodic and microcathodic regions on that surface, which preclude the need of another galvanically dissimilar metal in order to form a corrosion cell. Regarding the highly polished specimen surfaces used in this study, the effects of any such activity would be detrimental to data validity, especially when studied with a SEM. Consequently, to minimize corrosion not induced by the impressed current system, it was necessary to begin the experiment as soon as the assembly could be positioned in the tank solution. For tests involving a stationary anode, the desired value of impressed current was applied within 10 seconds of immersion. Under rotating conditions, the time elapsed was approximately 20 seconds because the necessary assembly rpm could not be achieved instantaneously. Note that in the latter case, no current was applied until anode velocity was stable, so as to avoid possible acceleration effects on the results.

As the corrosion circuit was completed, an electric timer was started. Timing accuracy available was up to 1/10th of a second, but according to the experimental plan, the length of each run was timed to within one second. Coinciding with the expiration of each time limit, the current generator was disconnected and the apparatus removed from the exposure tank as soon as possible. Analogous to the beginning of each test, the specimen remained submerged from 10 to 20 seconds depending on its stationary or rotating nature under impressed current conditions.

Once each corroded specimen was removed from the tank, but prior to being loosened from the disk slot setscrew, its surface was immediately rinsed with a gentle stream of distilled water. This procedure avoided damage to the corrosion product structure while thoroughly washing away the electrolyte. Failure to accomplish this would have resulted in an erroneous x-ray analysis of elements constituting corrosion products since some of the solution's chemicals would have remained on the metal surface. Specimens were subsequently removed from the slot, rinsed again, and allowed to dry naturally in air. A drying jet of freon gas could have harmed the corrosion product structure.

Once dried, each sample was mounted on a small aluminum stub which was designed to fit into a holder within the SEM chamber. The corroded metal surface was viewed at all useful magnifications available in an effort to characterize the effects of the various parameter combinations imposed according to experimental objectives. In addition, several scans

of elemental x-ray energies, emitted from regions displaying unusual or interesting surface corrosion features, were exhibited on the screen of the PGT 1000 analyzer for consideration. Figure 10 is an elemental x-ray presentation of the uncorroded sample pictured in Figure 9. The three distinctive peaks correspond to x-ray energies indicative of zinc.

Of course, both the SEM and x-ray analyzer were equipped to give the operator the ability to photograph video presentations, and most of the data collected for this work is in the form of these types of photographs. Figures included here substantiate salient observations and discussion concerning the effects studied.

Laboratory research was divided into several separate experiments, each designed to provide insights as to the effects of certain internal and external corrosion factors, namely anode velocity, current density, and current-time product. Table III lists each significant experimental set by its individual specimens, including which of the parameters were altered. Although a viable method of discussion would be to separately summarize the information gained according to each experiment, it is more fruitful to consider all of the data collectively since zinc anodic corrosion is dependent on a combination of factors. In many situations, such procedure proved essential for proper interpretation of results.

Determination of anode velocity relative to the electrolyte could not be exact. In spite of efforts to streamline the rotating disk assembly, solution disturbance was inevitable and steady state flow patterns developed within the tank

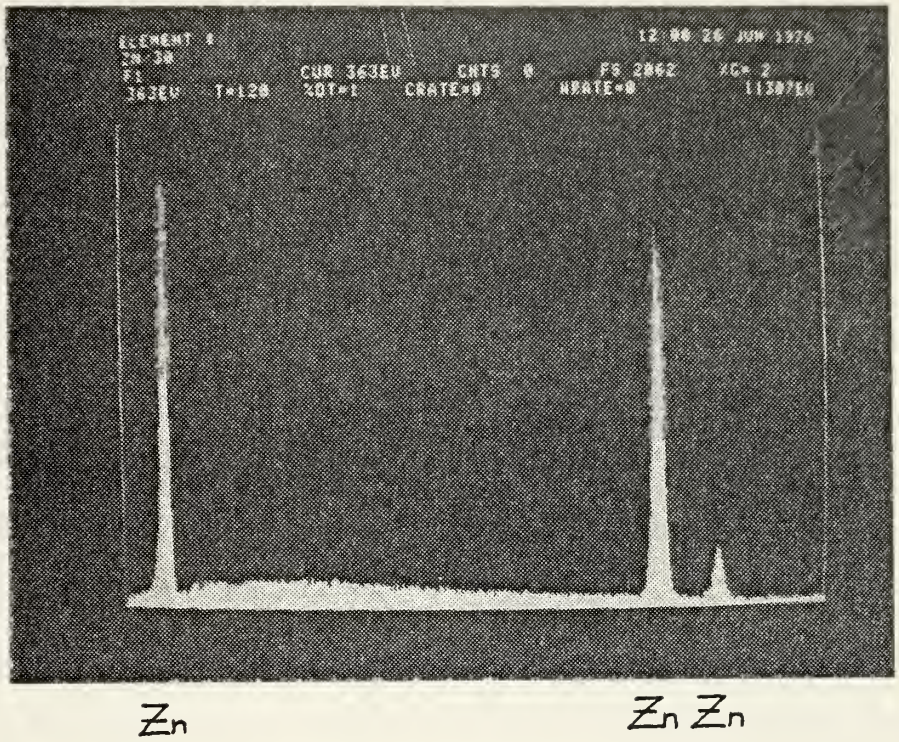

Figure 10

X-ray spectrum of clean zinc surface

during experimentation. In general, such patterns are inherent to all rotating mechanisms of this type, and cause fluid near the upper and lower disk surfaces to travel radially outward toward the disk periphery. To properly account for this phenomenon, it would be necessary to estimate the radial flow velocity near the zinc specimen slot and calculate the vector sum of this flow component and the disk tangential velocity (the product of the angular disk velocity (rpm) and the disk radius). Since radial flow patterns vary with disk angular velocity, a calculation for each disk speed used would be required. Complex mathematical formulas, which offer excellent correlation with experimental results, exist for this situation but the computational efforts involved here exceed the utility of such solutions as a matter of interest [25]. To simplify discussion, anode velocities are expressed relative to one another in terms of disk revolutions per minute.

Finally, it should be noted that for convenience, a 5-place alphanumeric code appears with each photograph presented in the analysis which references specimens to an individual experiment as listed in Table III. For example,"1ES10" denotes the tenth specimen (S10) in the first experiment (1E).

III. EXPERIMENTAL RESULTS AND DISCUSSION

A. VARYING ANODE VELOCITY

To provide basic insight concerning effects of velocity on the passivating mechanisms which affect contemporary shipboard zincs, a series of experiments was performed which simulated their actual operating environment. Here, individual specimens were subjected to a current density typical of in-service galvanic requirements while disk rpm were increased. In most cases, the exposure time of each specimen within the corrosive environment was held constant over a range of fixed anode velocities.

Figure 11 shows, at 26X, the surface of a zinc specimen having experienced a current density of 10 mA/in^2 (1.55 mA/cm^2) for 40 minutes at 30 rpm. Most obvious are the corrosion "streaks" which appear as diagonals due to combined effects of the radial and tangential velocity components, which are also indicated. The orientation of this photograph with respect to the velocity vectors shown is representative of subsequent figures used to illustrate these experimental results.

Each streak originates from an area having undergone a large amount of dissolution relative to the surrounding surface. Figure 12 is a picture of a dissolution area in greater detail. Figure 13 shows the presence of polishing scratches in an area upstream from such a site, indicating

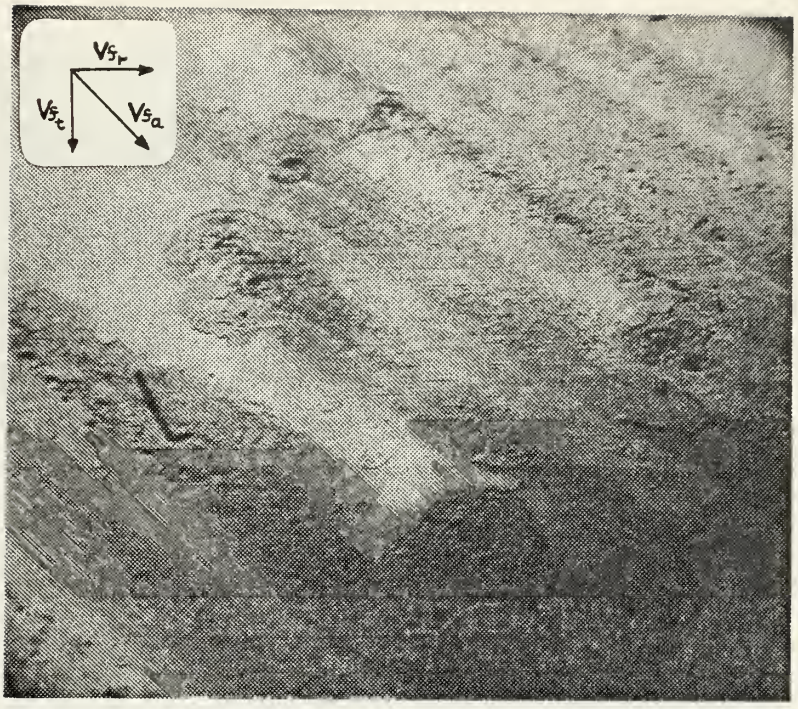

Figure 11

Zinc sample, 40 minute exposure at 10 mA/in^2 (1.55 mA/cm^2), 30 rpm, depicting large dissolution sites followed by corrosion product streaks. Vector Vf_t indicates direction of the tangential flow velocity component while Vf_r represents the radial flow component resulting from disk rotation. Vector Vf_a, the sum of Vf_t and Vf_r, is the direction of actual flow, relative to the specimen, 26X.
(3ES02)

Figure 12

Zinc sample, 40 minute exposure at 10 mA/in^2 (1.55 mA/cm^2), 30 rpm, showing large dissolution site, 75X
(3ES02)

Figure 13

Zinc sample, 40 minute exposure at 10 mA/in^2 (1.55 mA/cm^2), 75 rpm, showing unharmed upstream periphery of dissolution site, 610X
(3ES05)

relatively no attack. It is felt that each site of increased corrosion is caused by one or more microcathodic regions which enhance local current flow. This is supported by Figure 14 which is a typical x-ray spectrum of a heavily corroded site. In addition to the three characteristic zinc peaks in the spectrum, two additional energy peaks correspond to aluminum and lead. Todd showed several microcathodic lead inclusion sites where increased corrosion activity had occurred [22].

Figures 11, 15, and 16, which correspond to corrosion at disk rotations of 30, 75, and 90 rpm respectively, illustrate that moderate increases in velocity (at constant current-time product) affect the appearance of corrosion streaks in three ways. First, the number of streaks increases per unit of anode surface area. Secondly, individual streaks are more narrow. Finally, the surface sites where individual streaks initiate become smaller in diameter (less corrosive activity per streak). Clearly, at a fixed current density, an increase in the number of dissolution sites would indicate a decrease in the amount of corrosion per site, for a given time period, and give rise to narrower corrosion streaks. Reasons for increases in the number of dissolution sites are not intuitively obvious and warrant consideration.

Fluid dynamics seem to play an important role concerning changes in streak number and width. With each additional increment of rotational speed, electrolyte velocity gradients and thus local shear stresses on the specimen surface are increased. Such occurrences are caused by changes in the

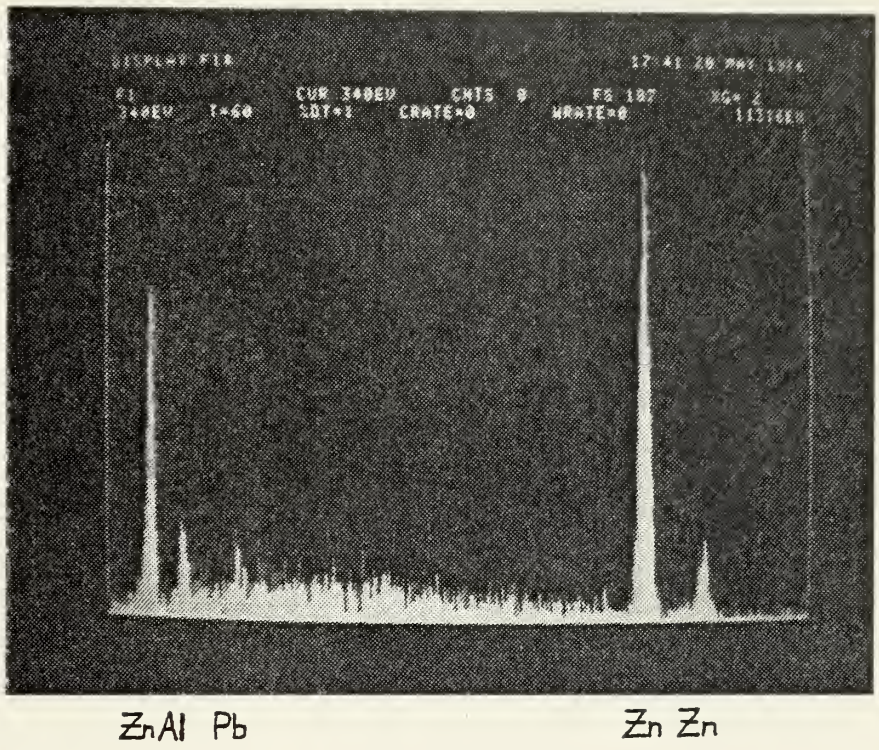

Figure 14

X-ray spectrum of dissolution site, 40 minute exposure at 10 mA/in^2 (1.55 mA/cm^2) 30 rpm
(3ES02)

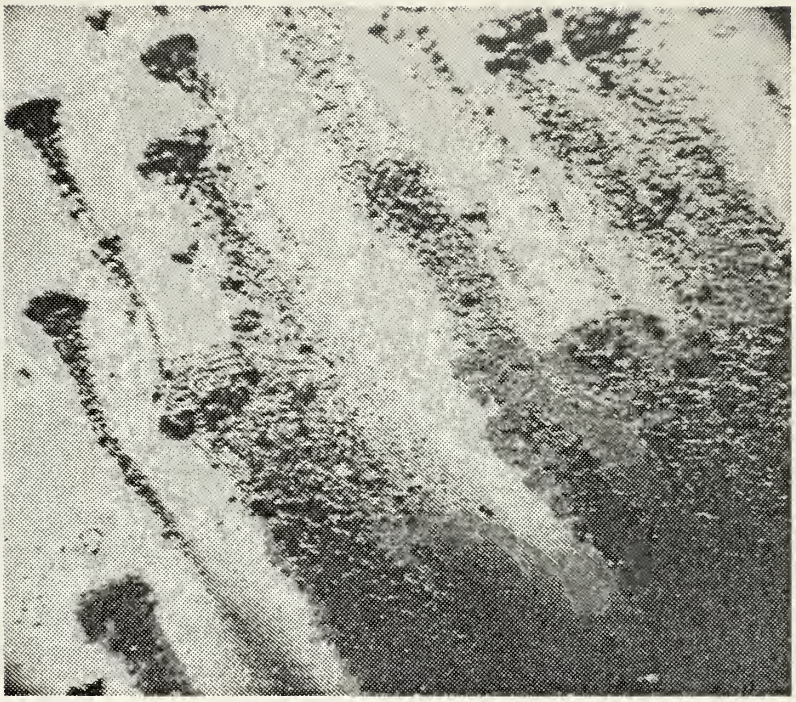

Figure 15

Zinc sample, 40 minute exposure at 10 mA/in^2 (1.55 mA/cm^2), 75 rpm, 26X
(3ES05)

Figure 16

Zinc sample, 40 minute exposure at 10 mA/in^2 (1.55 mA/cm^2), 90 rpm, 26X
(3ES06)

existing fluid boundary layer which constitutes a necessary interface between any moving object within a real and stationary fluid or alternatively, any stationary surface in a non-stationary fluid. Boundary layers account for the effects of fluid viscosity near the moving zinc anode surface in these experiments. Here viscosity causes the fluid next to the solid boundary to stick to the boundary so that no slippage or relative motion occurs. Moving away from the zinc, fluid velocity rapidly decreases in the boundary layer so that at the edge of the layer, the fluid is relatively motionless-having attained the free-stream characteristics of the environment.

Electrochemical factors can be modified in the event of a hydrodynamic boundary layer. Extensive discussions concerning fundamental electrode processes are offered by Gerisher and Petrocelli, who agree that electrode reactions are affected not only by concentration and chemical conditions, but also by the electrical conditions in and near the electrode/electrolyte boundary [23,25]. Near such an interface, oppositely charged particles accumulate as metal ions attempt to redistribute themselves to achieve an equal electrochemical potential between solid and solute metallic ions. Unequal currents exist as ions travel to and from the metal at different rates until equilibrium occurs (if ever). These currents cause the metal and the solution to become oppositely charged which results in an electrical double layer at the interface (due to charged particle accumulation). When equilibrium has been established, the electromotive force at the metal/solution

interface has been exactly counterbalanced by the electric potential difference formed between the phases as a result of the double layer [23]. The ability of ions to transfer from the metal surface through the double layer and into the solution, and vice versa, will determine the electromotive force of the corrosion reaction, while its rate is governed by the electrical potential difference between the metal/solution interface. This thermodynamic instability of the metal in the solution accounts for corrosion according to the mixed-potential theory which suggests that while separate cathodic and anodic sites on the metal surface can contribute to the process, they are not prerequisites [23].

Considering the observed increase in dissolution sites with increasing velocity, it is hypothesized that irregular removal of metallic ions to the hydrodynamic boundary layer occurs, leading to variable ionic concentration. The apparent dominance of physically microcathodic areas (related to base metal microstructure) under stationary conditions is thus reduced in more dynamic situations. To check the belief that dissolution sites in such situations are not dependent on the surface character of the anodes, small artificial pits and scratches were cut into a specimen surface with the tip of a regular straight pin, prior to corrosion. Figures 17 and 18 show the typical effects of a pit and scratch respectively. In Figure 17, a corrosion streak continues over and past the pit, apparently unaffected. A less pronounced streak passes over the scratch. The artificial grooves do not experience selective attack. The fact that some scratch dissolution

Figure 17

Man-made pit on zinc specimen, 40 minute exposure at 10 mA/in^2 (1.55 mA/cm^2) 30 rpm
125X
(4ES02)

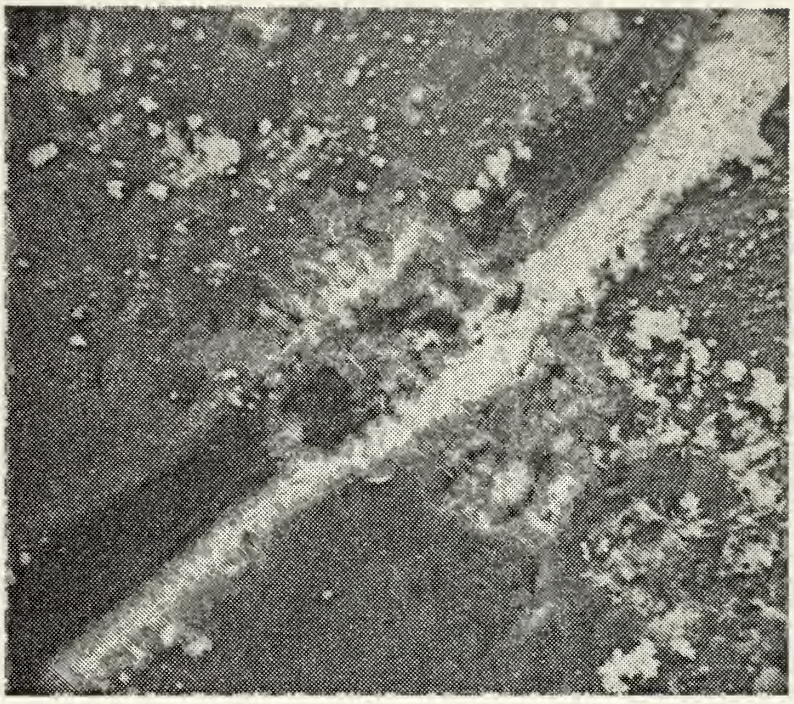

Figure 18

Man-made scratch on zinc specimen, 40 minute exposure at 10 mA/in^2 (1.55 mA/cm^2) 30 rpm, 320X
(4ES02)

occurred in the segment crossed by the streak suggests that the electrochemical nature of the streak's electrolyte sufficiently differs from that over unstreaked regions so as to cause dissolution of zinc along the entire streak.

The formation of ZnO (zinc oxide) platelets is said to depend on supersaturation of the electrolyte layer, immediately above the anode surface, with zinc ions [20, 21, 22]. Figure 19, which is greater magnification of the dissolution site shown in Figure 12, illustrates that supersaturation is still achieved in the vicinity of substantial corrosive activity in spite of the hydrodynamic boundary layer. The platelet structure appears to be identical to that obtained in static exposures by Todd. Figure 20 is a magnified view of the corrosion streak "downstream" from the above dissolution site. No platelets are visible but instead, an array of white corrosion products resembling cotton puffs appears. It is reasonable to expect that zinc ion concentration is lower in this region for two reasons: (1) ions are consumed upstream in formation of platelets and (2) ions are continually disbursed into the electrolyte. The implications are that zinc platelet nucleation is favored by higher ion concentrations and "cotton puff" formation is favored at lower ion concentrations.

Farmer and Webb have attempted to justify anodic zinc corrosion product dependence on electrolyte velocity with the aid of diffusion theory [26]. They offered that the appearance of a passivating film is dependent on a critical concentration of zinc ions at the electrode surface rather than in the electrolyte above it and that passivation thus depended on the

Figure 19

Dissolution site platelets on zinc specimen, 40 minute exposure at 10 mA/in^2 (1.55 mA/cm^2) 30 rpm, 2400X (3ES02)

Figure 20

Cotton puff corrosion products, downstream from dissolution site on zinc sample, 40 minute exposure at 10 mA/in^2 (1.55 mA/cm^2), 30 rpm, 1250X
(3ES02)

difference between the rate of ion formation and the subsequent rate of ion removal by the electrolyte. Ion transport from the surface is explained by the assumption of a hypothetical diffusion layer of electrolyte, of thickness δ, adjacent to the anode surface. A thick diffusion layer would inhibit ion removal and accelerate passivating film growth since ion diffusion rate is relatively slow.

Under laminar flow conditions (low electrolyte velocity relative to the zinc) the diffusion layer thickness, δ, is related to the hydrodynamic boundary layer thickness, δ_o, as:

$$\delta = \delta_o / Pr^{1/3} ,$$

where Pr is the Prandtl number associated with ion diffusion. In this particular electrolyte environment, $Pr \simeq 10^3$ so that:

$$\delta = 0.1 \, \delta_o .$$

The hydrodynamic boundary layer thickness in laminar flow over a flat surface is inversely proportional to the square root of the free-stream velocity so that both it and the diffusion layer decrease in thickness as the electrolyte (free-stream) velocity increases. Therefore, the critical ionic diffusion path and thus the passivation tendency will decrease with a relative increase in fluid velocity over the anode surface. Note that because of the inverse square root relationship, passivation time will become less and less sensitive to velocity changes. The experimental evidence presented by photographs in the present work appears to correlate with the

diffusion model predictions concerning ZnO platelet nucleation and/or deposition.

Because x-ray spectral analyses of several of the "cotton puff" products did not reveal the presence of elements other than zinc, the structure may represent another morphological state of ZnO. Since the products appear in the wake of dissolution sites, they apparently depend on zinc ion concentration in the electrolyte, but whether or not they originate within the electrolyte prior to settling, or form directly on the anode surface, has not been ascertained.

Concerning the extensive discussion on major sites of dissolution and the corrosion streaks which appear downstream from them, it should not be assumed that these are the only corrosive activities taking place. Figures 21, 22, and 23, photographs of surface regions between corrosion streaks, show that the activity of such areas can vary widely. They also point out that dissolution is not necessarily dependent on base metal microcathodic features.

As disk rpm was increased above 100, a drastic change in anode surface characteristics occurred. Figures 24 and 25 display this change at progressively higher magnifications. There was no evidence of corrosion streaks but instead, a compact, relatively uniform film covered the specimens. X-ray spectrum analysis of the film suggested that it may be yet another morphological form of zinc oxide.

The boundary layer formed at this disk speed is probably turbulent [27]. Turbulent boundary layers exhibit marked differences from laminar ones and cause regions of intense fluid

Figure 21

Secondary corrosive attack between streaks, zinc sample, 40 minute exposure at 10 mA/in^2 (1.55 mA/cm^2), 30 rpm, 660X
(3ES02)

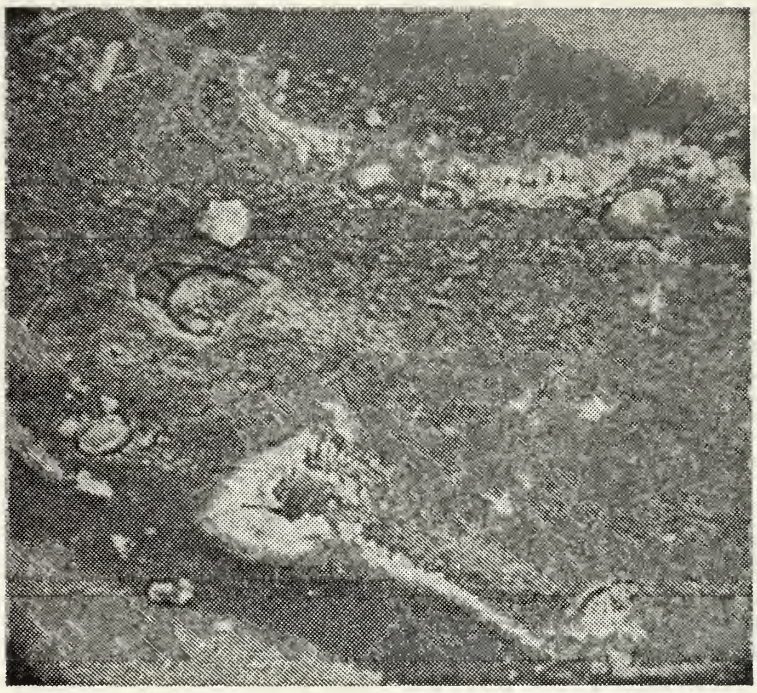

Figure 22

Secondary corrosive attack between streaks, zinc sample, 40 minute exposure at 10 mA/in^2 (1.55 mA/cm^2), 60 rpm, 255X
(3ES04)

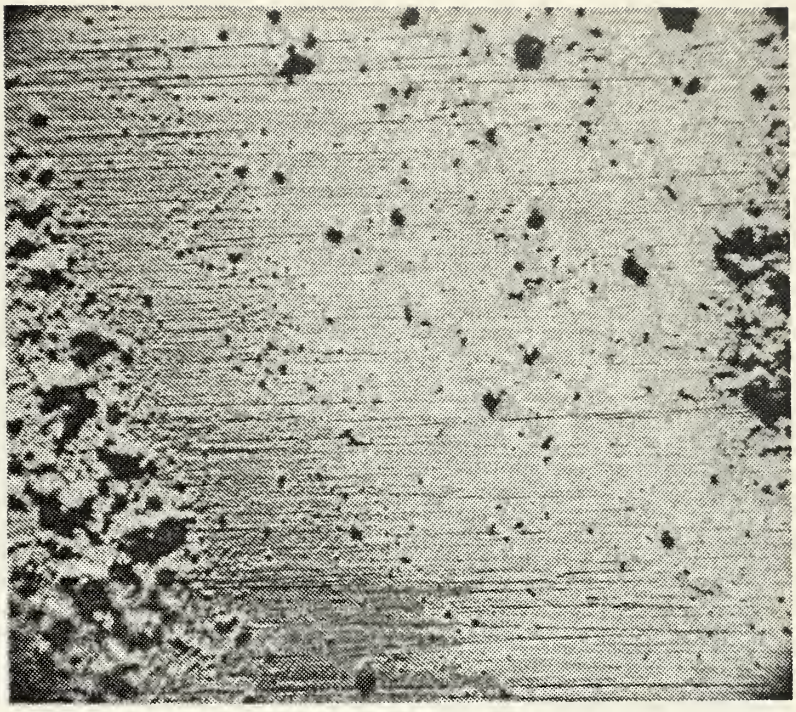

Figure 23

Zinc sample, 40 minute exposure at 10 mA/in^2 (1.55 mA/cm^2), 75 rpm, showing minor corrosive attack between streaks, 260X
(3ES05)

Figure 24

Zinc sample, 40 minute exposure at 10 mA/in^2 (1.55 mA/cm^2), 105 rpm, 67X (3ES07)

Figure 25

Zinc sample, 40 minute exposure at 10 mA/in^2 (1.55 mA/cm^2), 105 rpm, 670X (3ES07)

particle mixing and shear stress on the surface. Rapid dispersion of zinc ions is inevitable with turbulence so that electrochemical consequences are to be expected. Here, conditions dictate the limiting case concerning increases in the number of dissolution sites with increasing velocity, and individual dissolution sites have given way to more uniform surface attack in forming the zinc oxide film.

Several recent investigations of anodic zinc films in alkaline solutions (potassium hydroxide) have been reported [28,29,30,31]. In spite of electrolytic differences, experimental results using high purity (greater than 99.9%) zinc correlate with observances in the present study. Surface films identified as zinc oxide (by x-ray and electron diffraction) differed in form, depending to some extent on potential but with a major hydrodynamic influence. Under quiescent conditions, a loose, white, zinc oxide coating was observed, probably resulting from a precipitation mechanism, while when the electrolyte was stirred, they found that electrolyte supersaturation was prevented and a more compact, adherent zinc oxide film seemed to form directly on the zinc surface. An interesting auxiliary conclusion of this work indicated that following formation of a compact film, the majority of the current passed is utilized in direct electrochemical oxidation of the zinc to soluble products and not in further thickening of the surface layer [30].

The uniform appearance of the zinc oxide films formed at higher disk speeds initially suggested a tendency toward

passivation but further examination of the electrode surfaces indicated that this was not the case. Figure 26 shows an area where a portion of the film is absent, thus exposing more metal to the electrolyte. It is proposed that film removal was caused by two interacting processes, one of which is illustrated in Figure 27. Here a magnified view of the exposed metal surface from Figure 26 reveals a dense array of zinc oxide platelets. It is likely that they were able to nucleate and grow due to a thin electrolyte layer under the protective oxide film where velocity effects were nil. This correlates with the hypothesis explained above. As the platelets continued to form and grow, they may also have contributed to a loss of adherence of the compact film, leading to instability and cracking. Eventually the interacting process of the turbulent electrolyte removed the film. If this buildup/removal pattern were to continue cyclically, it is hypothesized that newly-exposed under-film platelets would become embedded in the following generation of compact zinc oxide film, while underneath this covering, platelet nucleation and growth would initiate another cycle, etc. It is considered that the cracks in the compact film do not conform to base metal grain boundaries for two reasons: the size of many cracked areas is in disagreement with the previously observed zinc anode grain size as defined by Todd in etched samples [22] and, additionally, numerous crack junction angles differ from 120°, the expected grain boundary junction angle.

The various effects of velocity observed so far have all been from specimens corroded at the experimentally determined

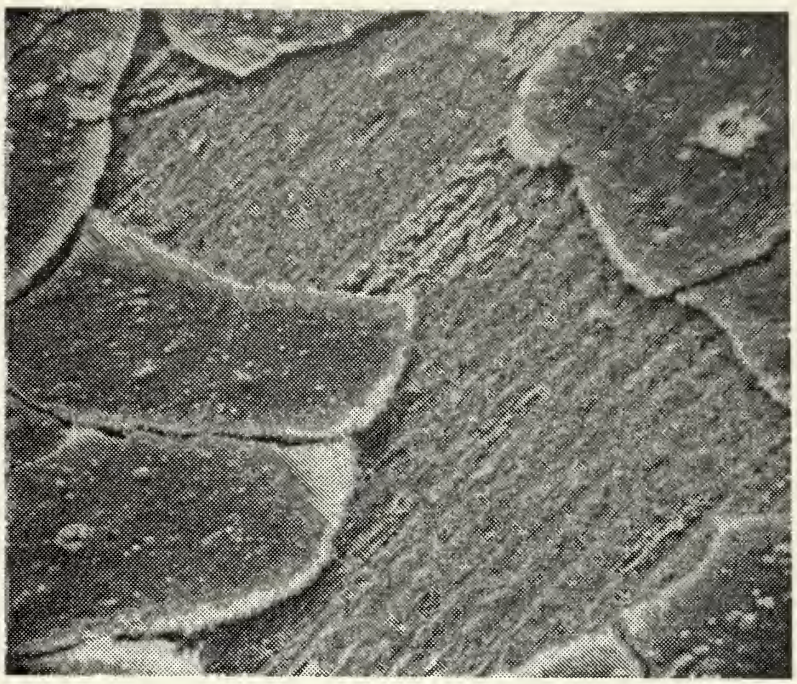

Figure 26

Fragmentation of compact zinc oxide film, revealing base metal surface of zinc sample, 40 minute exposure at 10 mA/in^2 (1.55 mA/cm^2), 105 rpm, 305X
(3ES07)

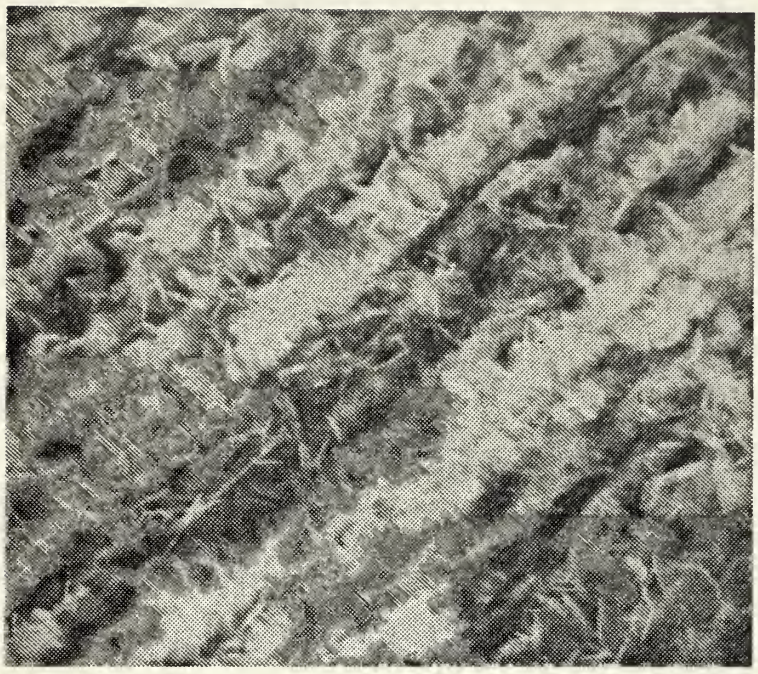

Figure 27

ZnO platelets on surface under compact zinc oxide film, zinc sample, 40 minute exposure at 10 mA/in^2 (1.55 mA/cm^2) 105 rpm, 3050X (3ES07)

"galvanic" current density of 10 mA/in^2 (1.55 mA/cm^2) for 40 minutes. Increasing the exposure time to 240 minutes produced some interesting results. Figure 28 shows a specimen surface held at the high speed of 130 rpm for the increased amount of time. The zinc oxide film is considerably more cracked and appears thicker. It is difficult to photograph because it is a poor conductor and reflects most of the SEM electrons, appearing "charged" and glowing. There were no exposed areas due to zinc oxide film removal. Compared to the 40 minute exposure, the cracks are much wider and allow observation of the base metal surface below. Figure 29 is a view "inside" a large crack and reveals the bare metal surface, showing crystallographic faceting. Electrolyte flow patterns in such a region are unknown but apparently dissolution of zinc without significant deposition of a corrosion product is occurring. Figure 30, taken over a different portion of the specimen, shows what appear to be conglomerate rows of corrosion product deposits on top of the cracked exterior film. These appear downstream of cracked film areas and are possibly the result of zinc dissolution ions available from within the upstream cracks. Figure 31 is a highly magnified view of such deposits.

Figure 32 exhibits the surface characteristics of a specimen corroded at a lower speed of 50 rpm, for the same time of 240 minutes. The direction of the electrolyte flow is obvious from corrosion product deposition just as in the case of the low-velocity specimens corroded for 40 minutes. This portion

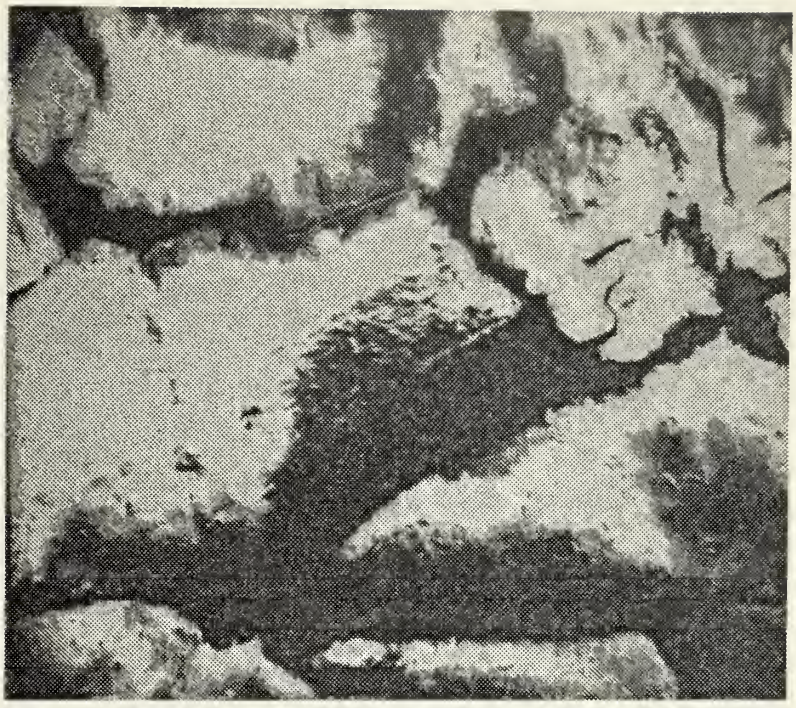

Figure 28

Zinc sample, 240 minute exposure at 10 mA/in^2 (1.55 mA/cm^2), 130 rpm, 84X (7ES06)

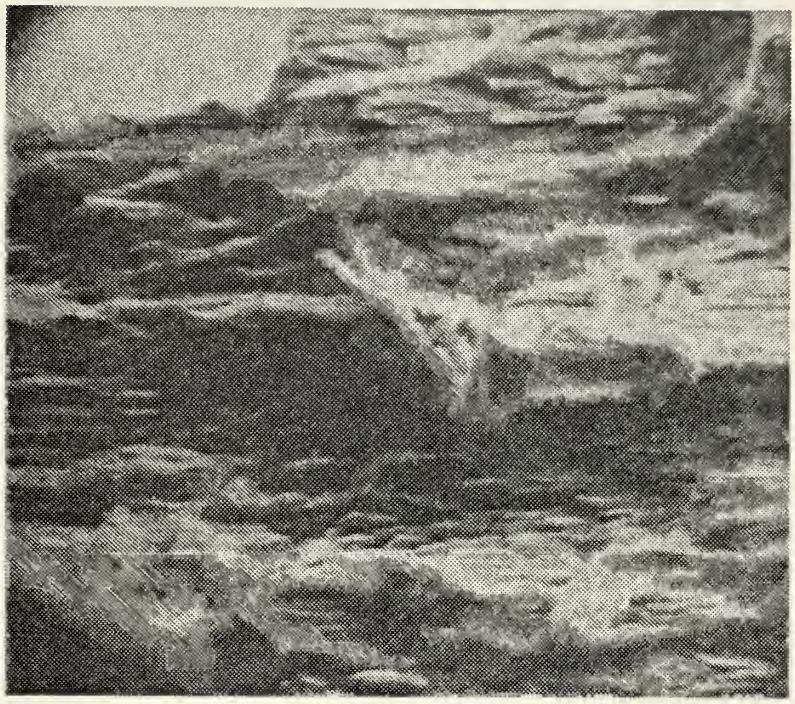

Figure 29

Metal surface under zinc oxide film crack, zinc sample, 240 minute exposure at 10 mA/ in^2 (1.55 mA/cm^2), 130 rpm, 1675X (7ES06)

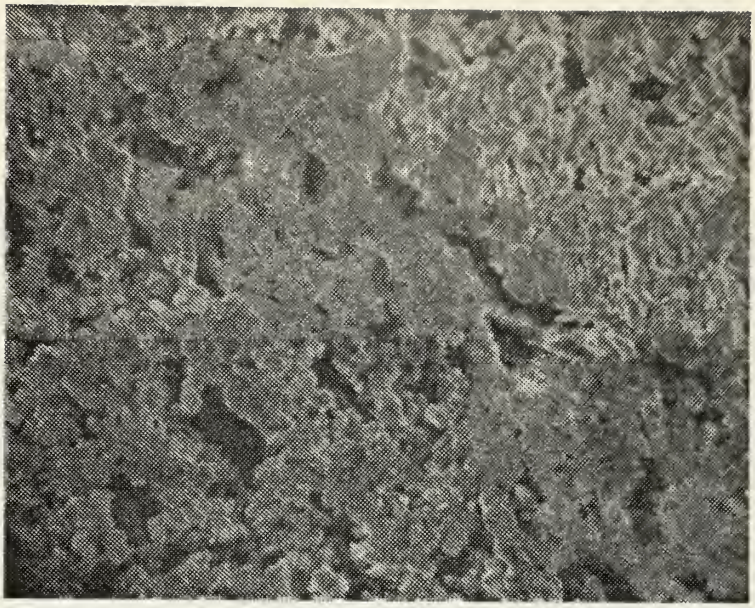

Figure 30

Conglomerate rows of zinc oxide deposits, zinc sample, 240 minute exposure at 10 mA/in^2 (1.55 mA/cm^2), 130 rpm, 295X
(7ES06)

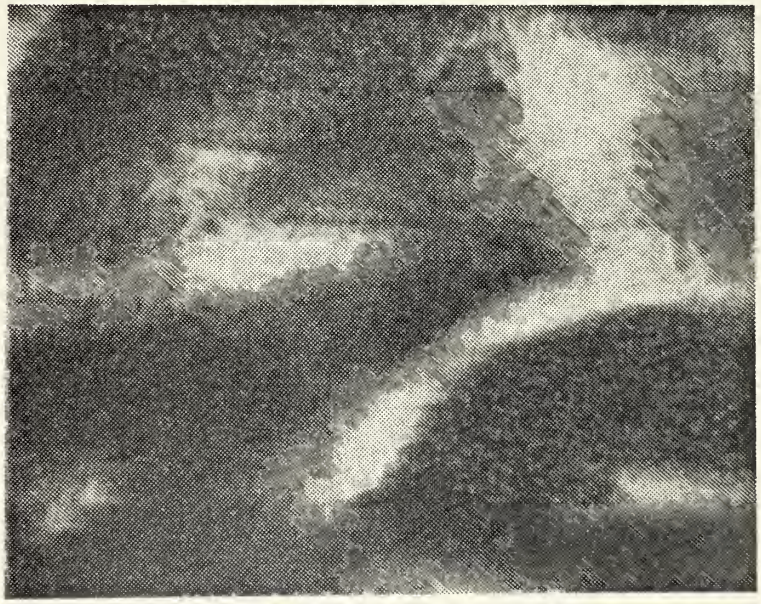

Figure 31

Zinc oxide deposits, zinc sample, 240 minute exposure at 10 mA/in^2 (1.55 mA/cm^2), 130 rpm, 8200X
(7ES06)

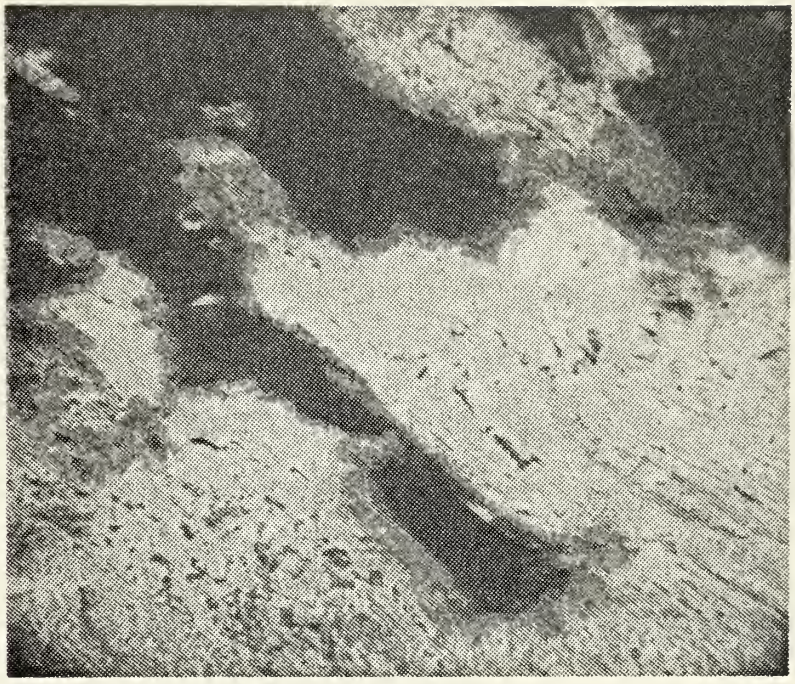

Figure 32

Zinc sample, 240 minute exposure at 10 mA/in^2 (1.55 mA/cm^2), 50 rpm, 125X (7ES07)

of the specimen "saw" the electrolyte first as it was rotated. Moving downstream over the surface, the deposits grew more dense because more zinc ions became available. Figure 33 illustrates the formation of cracks in this dense oxide film. Further downstream near the edge of the specimen, several pieces of the compact film have been removed to expose relatively bare metal with crystallographic faceting. Figures 34 and 35 reveal this phenomenon, the latter figure showing greater magnification of the exposed surface. The absence of a zinc platelets sublayer below the compact film suggests that the nature of the compact film formed slowly at low rpm values differs from the turbulent case. At lower velocities, it may be possible to form a slightly more coherent, adhesive structure (less fluid mixing and ion dispersion) under which no electrolyte sublayer would exist.

Reflecting on the results of these experiments and considering reports from Todd's previous study conducted under static conditions, it is obvious that velocity is a factor in the corrosion of anodic zinc. It has also been shown that specimens subjected to laminar and turbulent flow regimes exhibit markedly different features and that such differences may be explained by changes within the hydrodynamic and diffusion boundary layers. That higher velocities might lead to non-passivating anodes has been explained with a surface film buildup/removal model.

B. RIBBONLIKE CORROSION PRODUCTS

An interesting type of anodic corrosion product was observed on many specimens in this study that was not discussed by

Figure 33

Zinc sample, 240 minute exposure at 10 mA/in^2 (1.55 mA/cm^2), 50 rpm, 310X (7ES07)

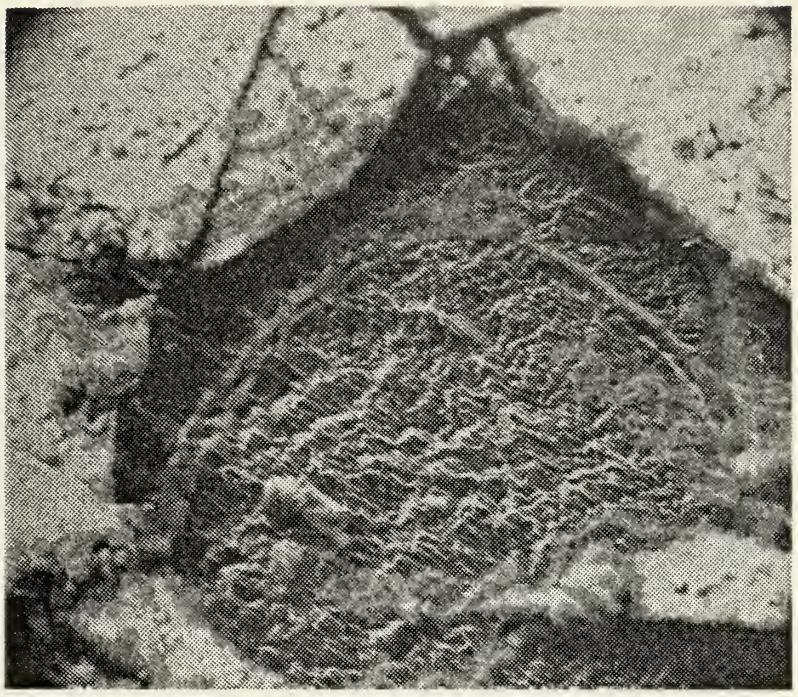

Figure 34

Surface under zinc oxide film, zinc sample, 240 minute exposure at 10 mA/in^2 (1.55 mA/cm^2), 50 rpm, 370X (7ES07)

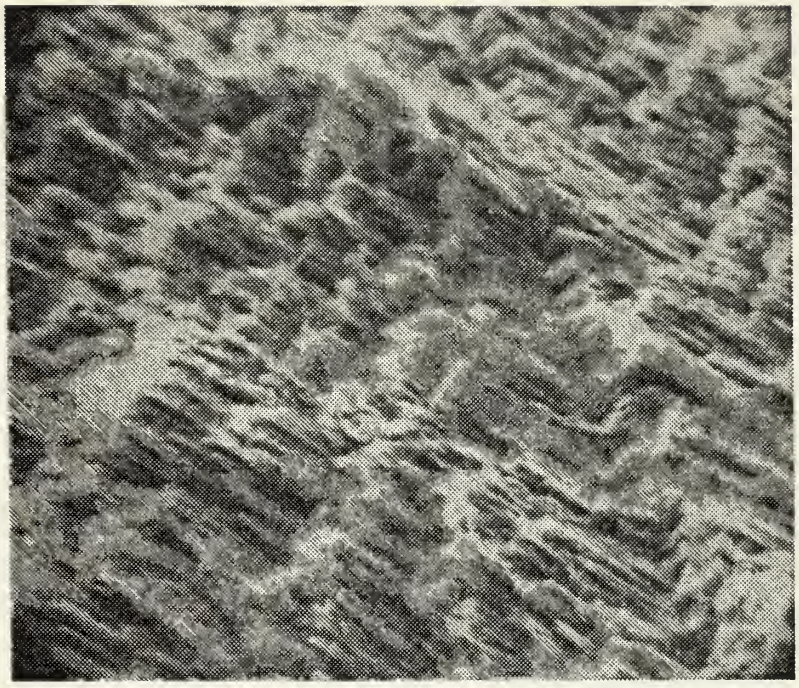

Figure 35

Surface under zinc oxide film, zinc sample, 240 minute exposure at 10 mA/in^2 (1.55 mA/cm^2), 50 rpm, 1850X (7ES07)

Bornholdt, Perkins, or Todd [19,20,21,22]. It can be described as a white, ribbonlike structure which generally encircles a small amount of surface area. X-ray spectrum analyses of a number of such structures on various specimens did not indicate that composition differed from zinc oxide and therefore, it was assumed to be another morphological form of this compound. Figure 36 vividly portrays these characteristic ribbonlike enclosures. The conditions necessary for their formation warrant discussion.

Zinc oxide ribbon formation appears to be dependent on local electrochemical conditions at the base metal zinc surface. They are only indirectly affected by anode velocity, in the sense that velocity can alter the local electrochemical environment. Alternatively, when the local electrochemical environment is governed predominantly by a base metal microcathodic feature, such as an inclusion, and is relatively unaffected by anode velocity, factors leading to ribbon deposition are realized. Figure 37 shows corrosion resulting from a disk speed of 45 rpm, at the experimentally determined current density, for 40 minutes. The fact that some ribbons encircle dissolution sites (probably inclusions) while others form along streak boundaries, justifies the above statements.

To gain more knowledge about the initial stages of ribbonlike zinc oxide formation, several specimens were kept stationary and subjected briefly to very low current densities. Figures 38 and 39 were taken of specimens corroded statically for 2 minutes at current densities of 0.5 mA/in^2 (0.0775 mA/cm^2) and 1 mA/in^2 (0.155 mA/cm^2) respectively. These current-

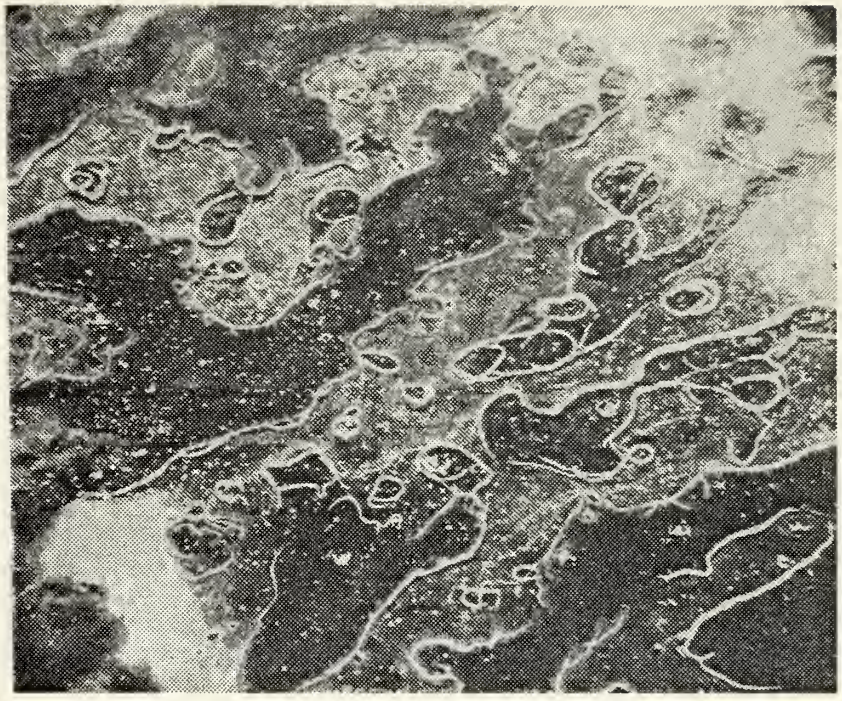

Figure 36

Ribbonlike structures on zinc sample, 5 minute exposure at 5 mA/in^2 (0.775 mA/cm^2), 15 rpm, 65X (1ES01)

Figure 37

Zinc sample, 40 minute exposure at 10 mA/in^2 (1.55 mA/cm^2), 45 rpm, 28X (3ES03)

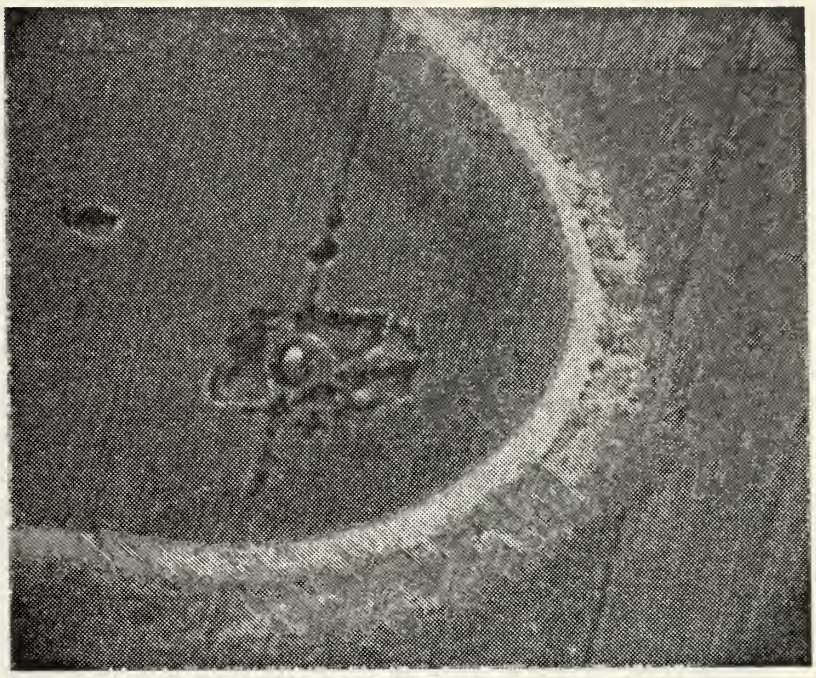

Figure 38

Zinc sample, 2 minute exposure at 0.5 mA/in^2 (0.0775 mA/cm^2), stationary, 1300X (6ES07)

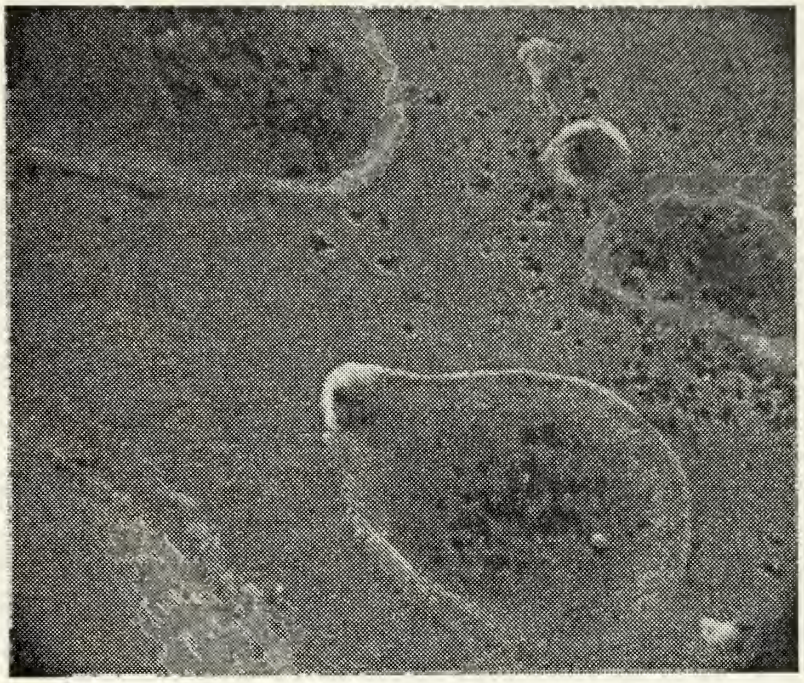

Figure 39

Zinc sample, 2 minute exposure at 1 mA/in^2 (0.155 mA/cm^2), stationary, 640X
(6ES05)

time products are much less than those necessary for platelet nucleation and growth, but the ribbonlike products are present. It is significant to note that they only encircle relatively pitted or more anodic areas where dissolution rates are highest. Note that no specific microcathodic features are visible at the center of the pitted regions of Figure 39. However, in some cases, such as Figure 40, an apparent microcathodic region is encircled by the ribbon (ribbon not shown). Figure 41 is the x-ray spectrum of this microcathode, which indicates the presence of a lead inclusion.

Growth of zinc oxide ribbons usually continues until zinc oxide platelets begin to form. Using the low current density of 0.5 mA/in^2 (0.0775 mA/cm^2) for a much longer time of 30 minutes, the ribbons enclosing the area of small pits and platelets, shown in Figure 42, were as developed as any observed throughout the study. It is hypothesized that the causative factor for such growth is a type of anodic/cathodic interface, outside of which zinc oxide platelet deposition is severely inhibited in the early stages of exposure. Figures 43 and 44 support the hypothesis by illustrating zinc oxide platelet nucleation near these boundaries. Platelet formation is abruptly less pronounced outside the ribbon-encircled areas. Therefore, it appears that the local influences which favor ribbon formation remain even after ribbon development has apparently ceased. In addition, the existence of zinc oxide ribbons was not found to be dependent on current density.

Figure 40

Microcathodic region encircled by zinc oxide ribbon (ribbon not shown), zinc sample, 2 minute exposure at 0.5 mA/in^2 (0.775 mA/cm^2), stationary, 2600X (6ES07)

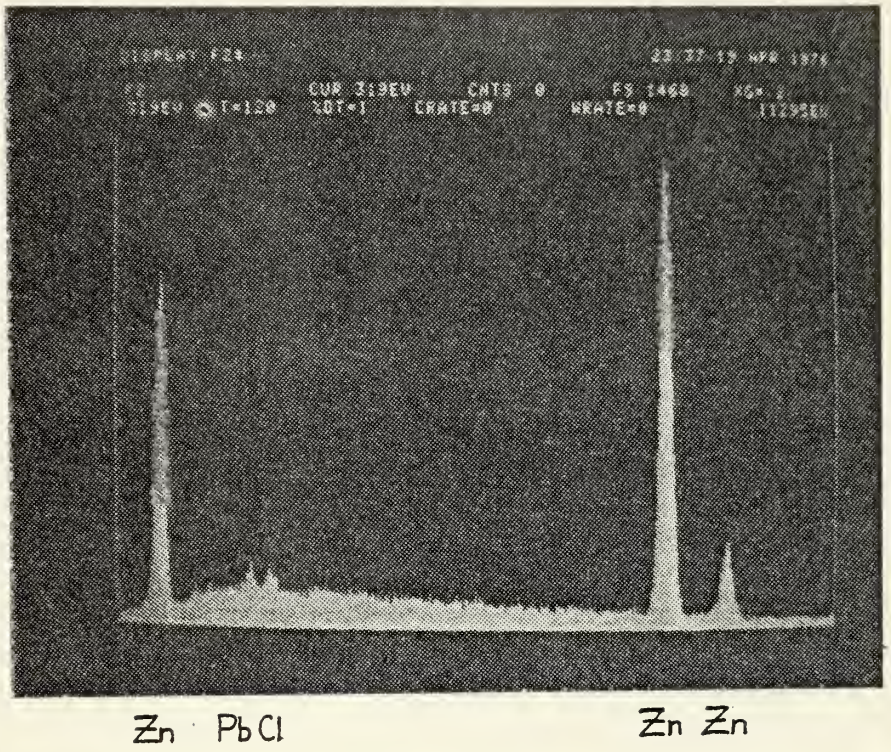

Figure 41

X-ray spectrum of microcathodic region zinc sample, 2 minute exposure at 0.5 mA/in^2 (0.775 mA/cm^2), stationary (6ES07)

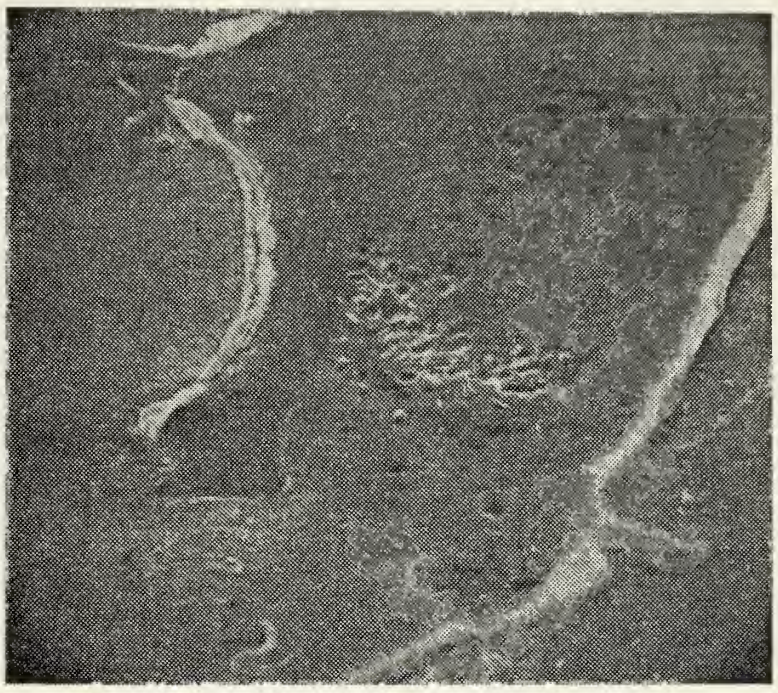

Figure 42

Zinc sample, 30 minute exposure at 0.5 mA/in^2 (0.0775 mA/cm^2), stationary, 280X (6ES09)

Figure 43

ZnO platelet behavior at ribbonlike boundary, zinc sample, 40 minute exposure at 10 mA/in^2 (1.55 mA/cm^2), 60 rpm, 2500X
(3ES04)

Figure 44

ZnO platelet behavior at ribbonlike boundary, zinc sample, 40 minute exposure at 10 mA/in^2 (1.55 mA/cm^2), 60 rpm, 2500X
(3ES04)

To define the structure of these ribbons, one must go to very high magnifications, where the structure appears as a dense, homogeneous mass, speckled with tiny zinc oxide platelets (Figure 45). It is possible that in time larger platelets evolve from this structure. A likely evolution process is presented in Figures 45, 46, 47, 48, and 49 which support this possibility. Note that in Figures 48 and 49, the hypothetical anode-cathode interface is no longer prevalent; platelets appear on both sides of the former boundary.

C. VARYING CURRENT DENSITY

Further deviation from the experimentally determined current density of 10 mA/in^2 (1.55 mA/cm^2) was undertaken to study the effects of this corrosion factor under several environmental conditions. The product of current density and exposure time used for each specimen, the current-time product, provided a useful scale for corrosion comparisons.

By their very nature, electrochemical mechanisms are strongly dependent on the flow of electrical current. Other things equal, an increase in current density on an anodic surface will increase ion dissolution rate and thus factors related to higher concentrations of solute ions are affected. This relationship was easily seen by making drastic variations in current density while keeping exposure times of 2 minutes per specimen. Figures 50, 51, and 52 correspond to densities of 0.5, 1.0, and 50. mA/in^2 (0.0755, 0.155, and 7.75 mA/cm^2) respectively, under stationary conditions. Most notable with increasing current density was the tendency

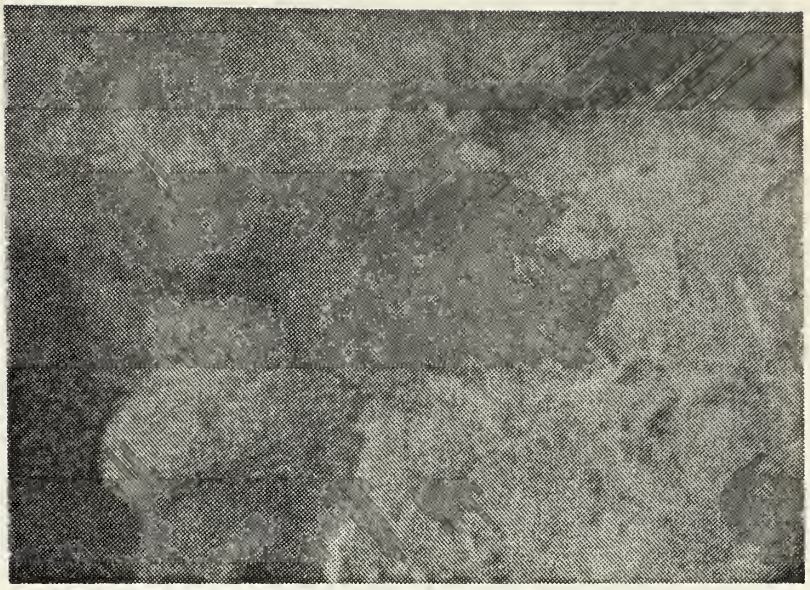

Figure 45

Ribbonlike structure, zinc sample, 40 minute exposure at 10 mA/in^2(1.55 mA/cm^2), 60 rpm, 6200X
(3ES04)

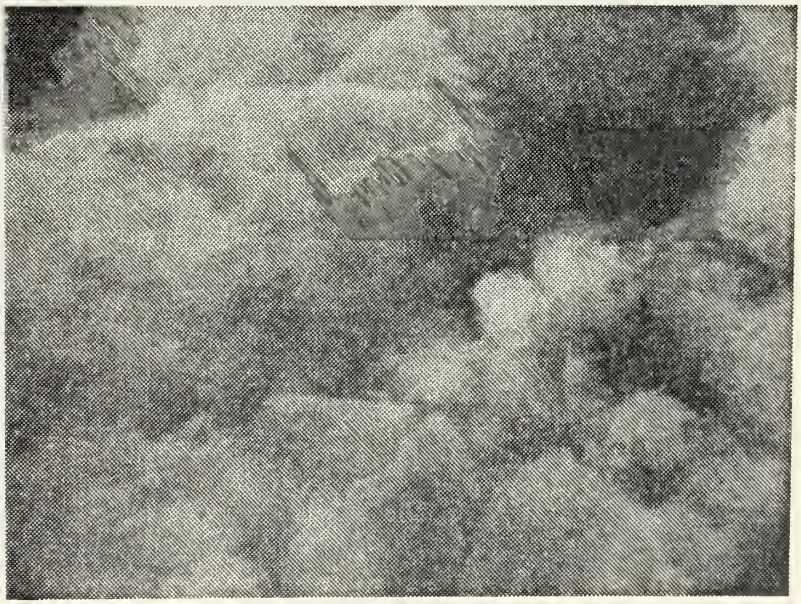

Figure 46

Ribbonlike structure, zinc sample, 8 minute exposure at 50 mA/in^2(7.75 mA/cm^2), stationary, 7900X
(7ES03)

Figure 47

Ribbonlike structure, zinc sample, 40 minute exposure at 10 mA/in^2(1.55 mA/cm^2), 60 rpm, 6400X
(3ES04)

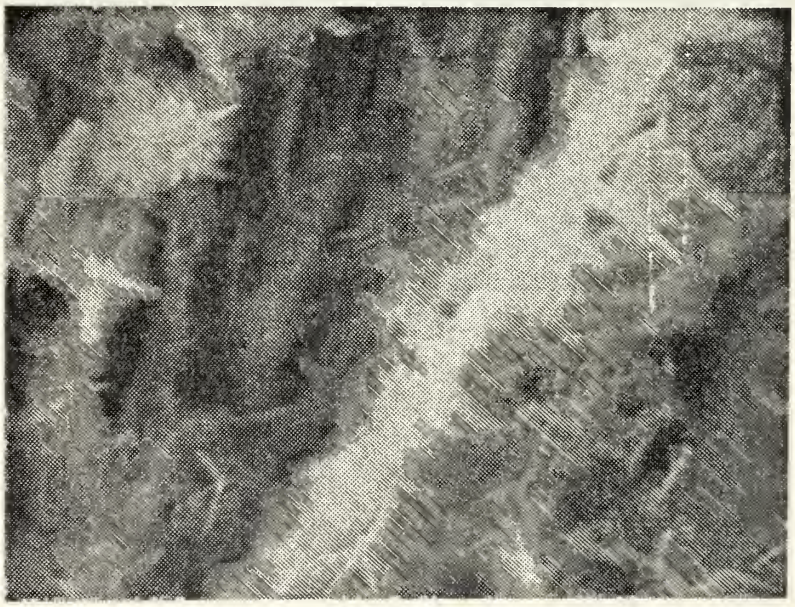

Figure 48

Ribbonlike structure, zinc sample, 40 minute exposure at 50 mA/in^2(7.75 mA/cm^2), stationary, 3100X
(7ES01)

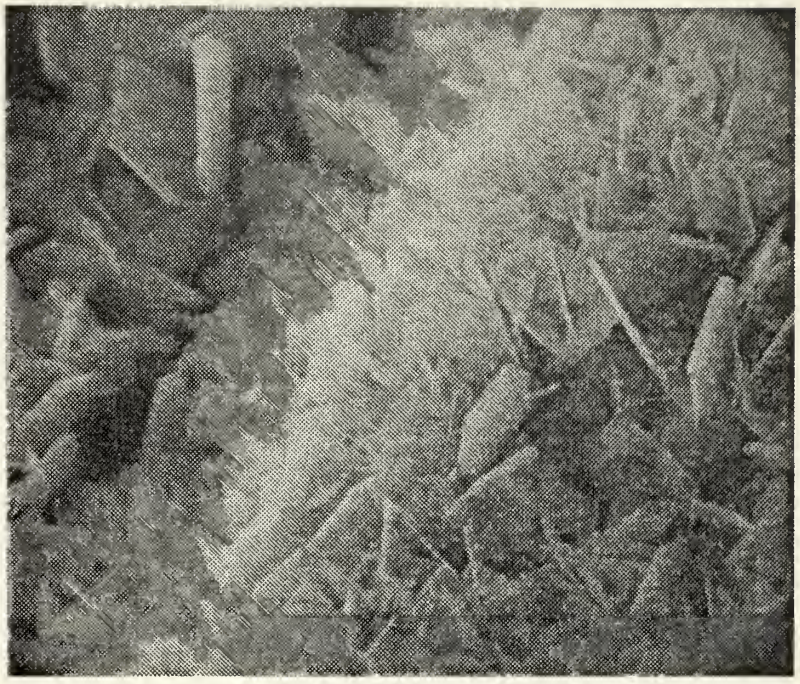

Figure 49

Possible former ribbonlike structure, zinc sample, 120 minute exposure at 50 mA/in^2 (7.75 mA/cm^2), stationary, 1650X (7ES02)

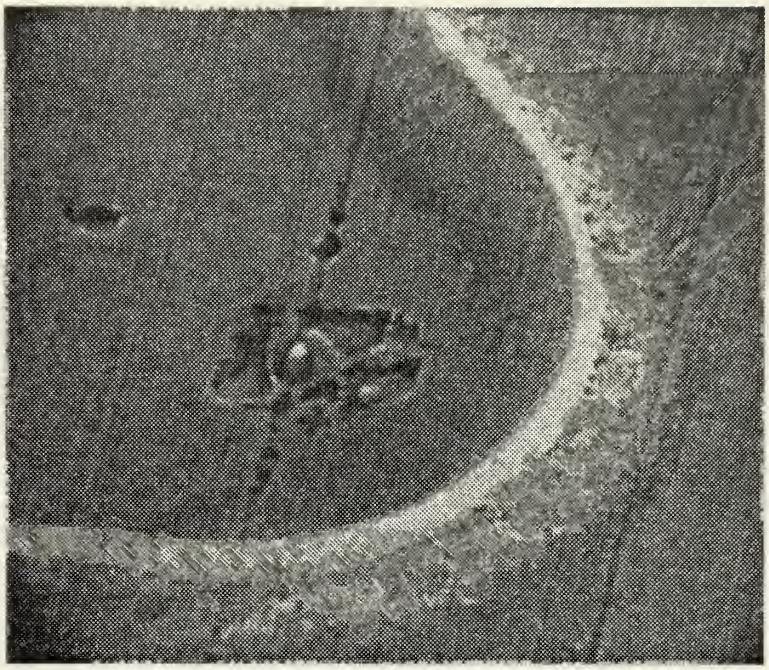

Figure 50

Zinc sample, 2 minute exposure at 0.5 mA/in^2 (0.0775 mA/cm^2), stationary, 1300X
(6ES07)

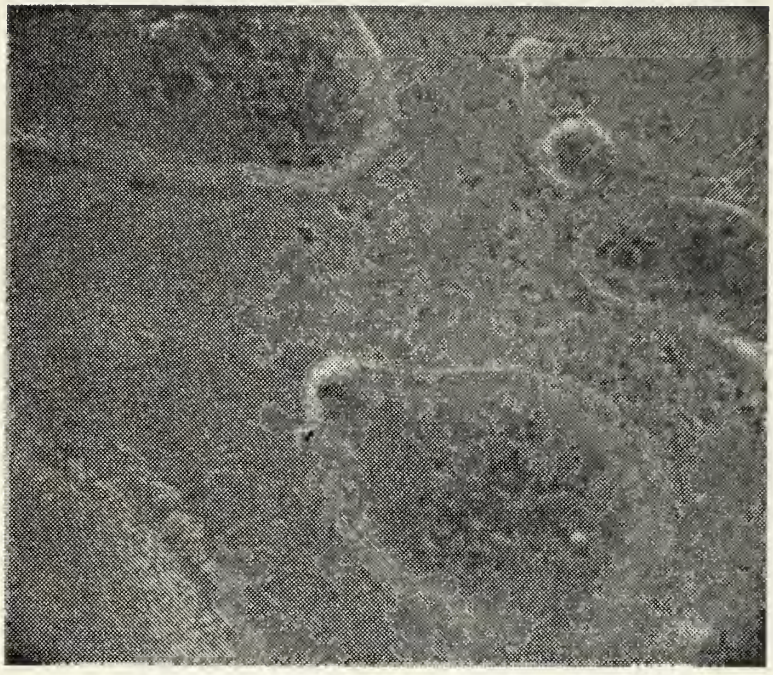

Figure 51

Zinc sample, 2 minute exposure at 1 mA/in^2 (0.155 mA/cm^2), stationary, 640X
(6ES05)

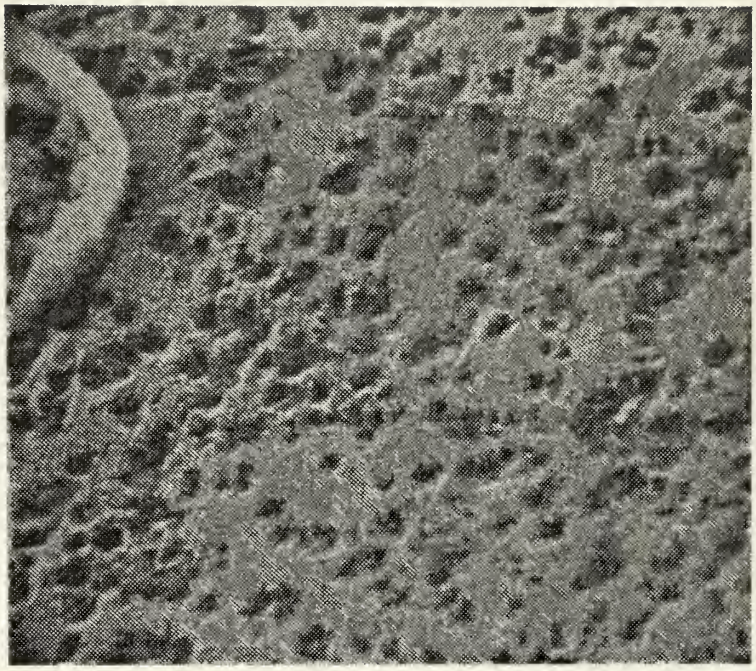

Figure 52

Zinc sample, 2 minute exposure at 50 mA/in^2 (7.75 mA/cm^2), stationary, 875X (7ES04)

toward more dissolution sites per unit area and therefore more uniform dissolution.

Todd reported that ZnO platelet nucleation occurred in approximately 10 minutes using his galvanic apparatus [22]. Assuming that the estimated anodic current density of 10 mA/in^2 (1.55 mA/cm^2) was operable for the Todd setup, then platelets should be observed with a current-time product equal to or greater than 100 mA•min/in^2 (15.5 mA•min/cm^2)(zero anode velocity). The current-time product corresponding to the specimen in Figure 52 was exactly 100 mA•min/in^2 (15.5 mA•min/cm^2), but used five times the current density with one-fifth the amount of time corresponding to conditions in Todd's case. Figure 53 is a highly magnified view of a typical pit on the specimen showing several tiny (1.5 μm) ZnO platelets, thus confirming a dependence on the current-time product rather than each factor separately. The notion of platelet dependence on ion concentration is also supported here since initial platelets only appeared in high-dissolution sites such as pits.

With a moderate increase in exposure time to approximately 30 minutes, the results of current density differences are equally dramatic. Although the lengths of exposure differed by 25%, specimens shown in Figures 54 and 55 clearly illustrate the effects of a 100-fold variation in current density (0.5 mA/in^2 (0.0775 mA/cm^2) for 30 minutes vs. 50 mA/in^2 (7.75 mA/cm^2) for 40 minutes). Note also the white cluster deposits in Figure 55. According to Todd, such structures preceded

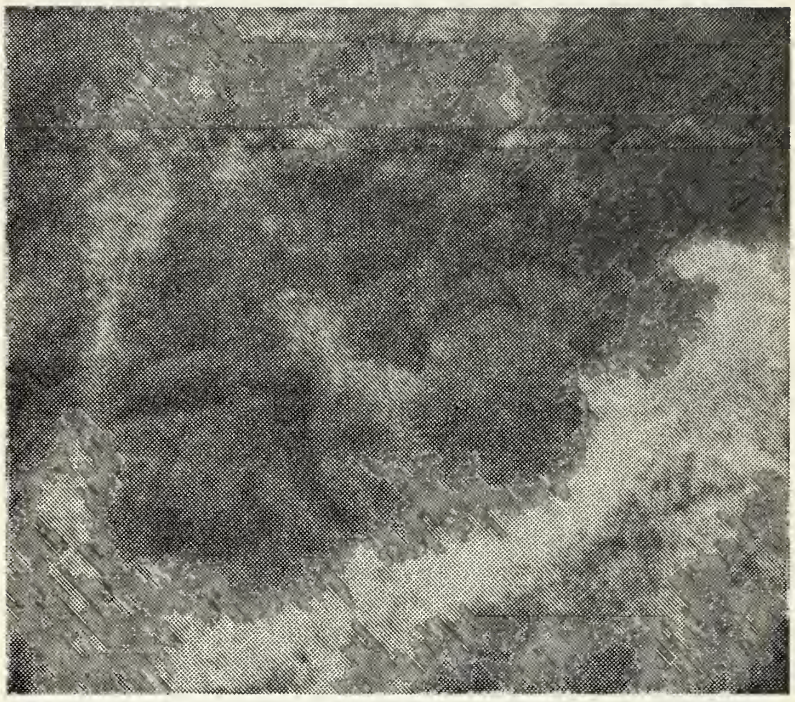

Figure 53

Tiny ZnO platelets in pit, zinc sample, 2 minute exposure at 50 mA/in^2 (7.75 mA/cm^2), stationary, 8750X (7ES04)

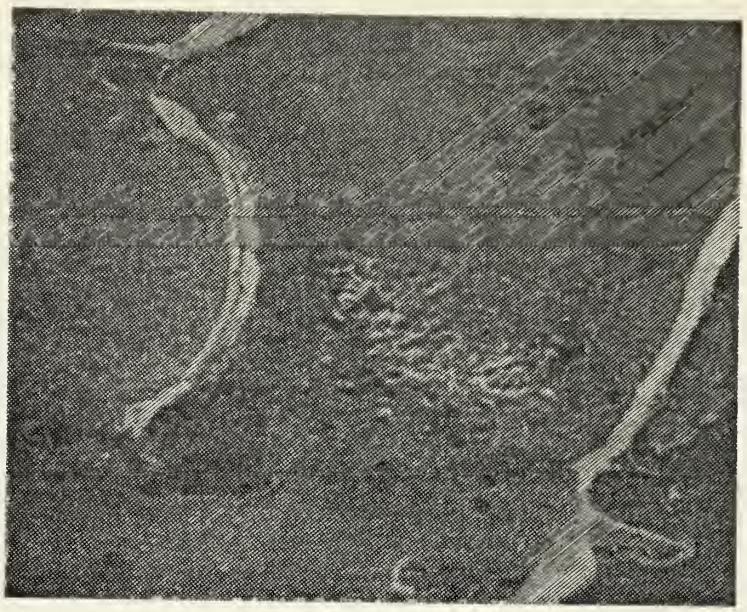

Figure 54

Zinc sample, 30 minute exposure at 0.5 mA/in^2 (0.0775 mA/cm^2), stationary, 280X (6ES09)

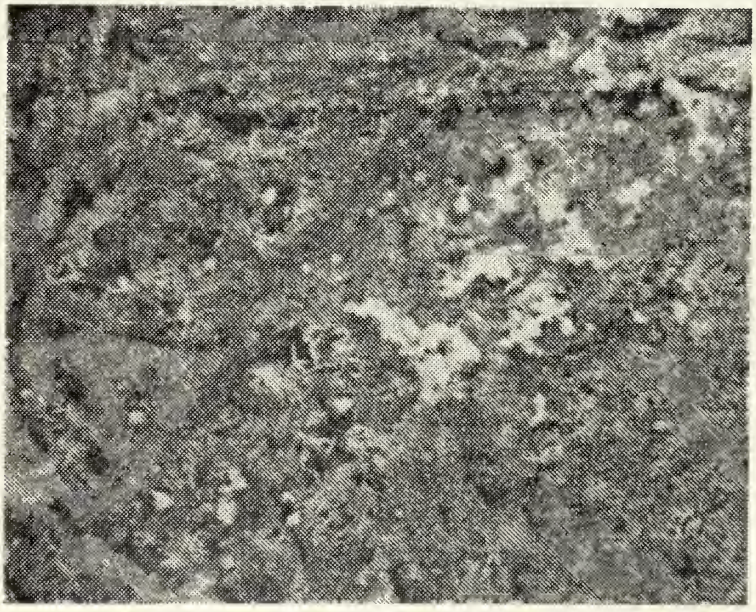

Figure 55

Zinc sample, 40 minute exposure at 50 mA/in^2 (7.75 mA/cm^2), stationary, 310X (7ES01)

anode passivation and appeared after approximately 4 hours exposure, usually located over microcathodic areas. Figure 56 shows one cluster in greater detail. Similar to the role played in individual ZnO platelet formation, these results show that appearance of the cluster oxides is also dependent on attainment of a sufficient current-time product. As with the platelets, current density was five times the apparent galvanic value of the Todd experiments, applied for only one-fifth the galvanic exposure time.

Several noteworthy observations were made following experiments in which each specimen was subjected to a different current density for a relatively long period of time. When current densities were kept less than or near the assumed natural galvanic value of 10 mA/in.^{2} (1.55 mA/cm^2) for 4 hours, small regions on each specimen were covered with ZnO platelets oriented parallel to the metal surface, i.e., Todd's hypothetical passivation mechanism [22]. Interestingly though, higher current densities for the same amount of time did not produce any such passivating areas; a layer of larger platelets appeared to grow over the existing network platelet structure but neither layer exhibited the parallel growth pattern; the larger platelets were not regularly hexagonal and in some instances their diameters measured 0.0071 in (180 μm)-over 3½ times the maximum size reported in the previous study [22].

Figures 57 and 58 were taken of a specimen that had undergone 5 mA/in^2 (0.775 mA/cm^2) current density for 4 hours. The upper right corner of the first photograph shows some plate-

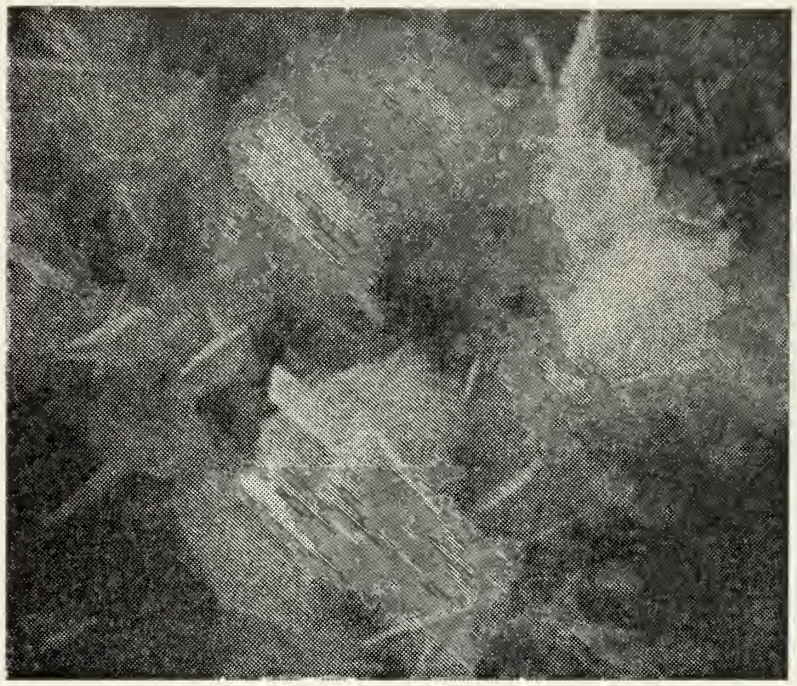

Figure 56

ZnO platelet cluster, zinc sample, 40 minute exposure at 50 mA/in^2(7.75 mA/cm^2), stationary, 3100X
(7ES01)

Figure 57

Zinc sample, 240 minute exposure at 5 mA/in^2 (0.775 mA/cm^2), stationary, 90X (8ES01)

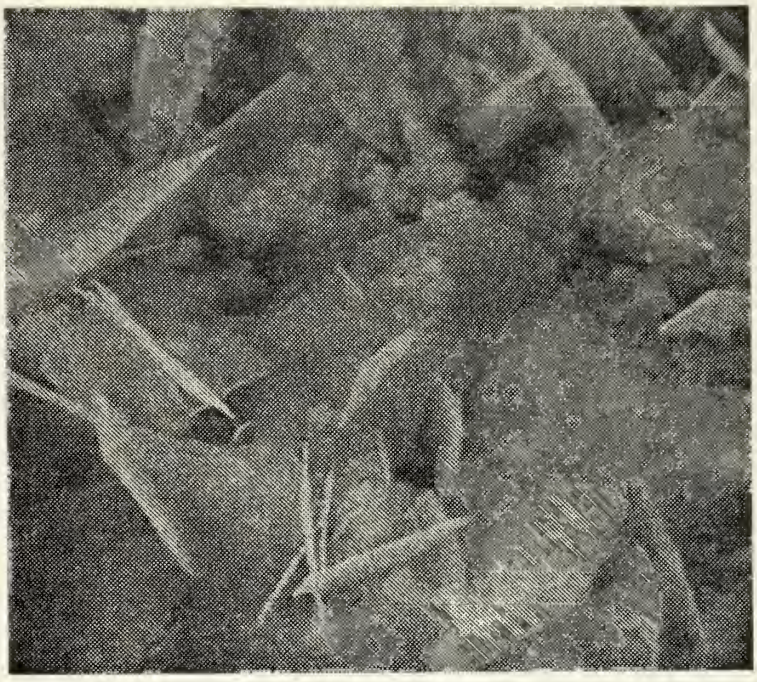

Figure 58

Film growth on zinc sample, 240 minute exposure at 5 mA/in^2 (0.775 mA/cm^2), stationary, 1500X
(8ES01)

lets embedded in a dark, film-like layer. The latter reveals that this layer is partially composed of ZnO plates having grown parallel to the surface. Since some ZnO platelets continue to grow on top of the parallel layer, this suggests that it does not constitute complete passivation. Figures 59 and 60 reveal two similar areas on a specimen corroded at 10 mA/in^2 (1.55 mA/cm^2) for 4 hours (twice the current density for the same time of the preceding specimen). The increased current caused more numerous ZnO platelets in the non-passivating region while the parallel platelet layer appeared more coherent. The proportion of "passivated surface" on each specimen was approximately the same.

Figures 61, 62, and 63 correspond to 4-hour exposures at current densities of 20, 30, and 50 mA/in^2 (3.10, 4.65, and 7.75 mA/cm^2) respectively. Development of a second layer of larger platelets with increasing current-time product is obvious. Maximum plate diameter in the last photograph was nearly 0.0028 in (70 μm). A final experiment using a current density of 20 mA/in^2 (3.10 mA/cm^2) for 15 hours failed to produce any passivating layer. As shown in Figure 64, platelets grew in an irregular fashion to very large diameters (0.0071 in (180 μm)). Although it was not determined if the "passivating" layers were subsequently masked by continued surface growth on these higher current density exposures, consideration of the platelet growth seen in Figure 57 indicates that such a process might occur. Further experiments on stationary specimens, beyond this range of current-time products,

Figure 59

Zinc sample, 240 minute exposure at 10 mA/in^2 (1.55 mA/cm^2), stationary, 850X (7ES05)

Figure 60

Zinc sample, 240 minute exposure at 10 mA/in^2 (1.55 mA/cm^2), stationary, 1400X (7ES05)

Figure 61

Zinc sample, 240 minute exposure at 20 mA/in^2 (3.10 mA/cm^2), stationary, 850X (8ES02)

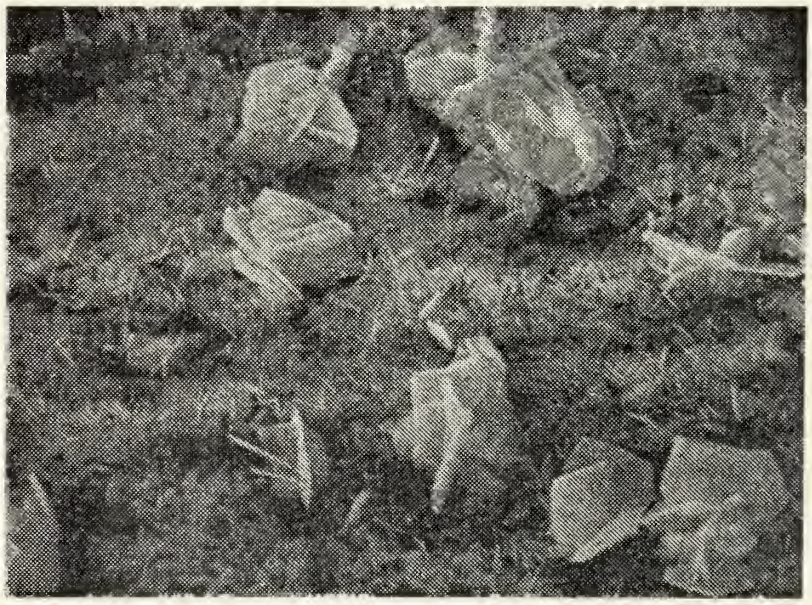

Figure 62

Zinc sample, 240 minute exposure at 30 mA/in^2 (4.65 mA/cm^2), stationary, 320X (8ES03)

Figure 63

Zinc sample, 240 minute exposure at 50 mA/in^2 (7.75 mA/cm^2), stationary, 180X (8ES05)

Figure 64

Zinc sample, 900 minute exposure at 20 mA/in^2 (3.10 mA/cm^2), stationary, 140X (8ES06)

were not conducted. It was thought that further divergence from shipboard galvanic conditions was unwarranted.

Considering the kinetic origin of passivation effects, Conway [33] suggests that the phenomenon can begin in two or three distinguishable ways: (1) alteration of the effective surface area exposed to the electrochemical environment; (2) modification of the electrochemical standard free energy of activation; or (3) a change in the local field at the surface of the electrode, even if only by a small amount of surface coverage. He qualifies the effect of (3) as being like (2) but possibly more specific and acting under less surface coverage (by corrosion products)[33]. Accepting Todd's hypothesis that mechanism (3) is applicable to zinc passivating tendencies, it is further hypothesized that dominant impressed fields, greater in magnitude than those produced in natural galvanic couples, effectively prevented local field changes necessary for passivation in this particular environment. It is likely that dissolution and platelet growth on stationary specimens would continue until the semiconductive characteristics of such products were able to override the formidable electromotive force.

At this point, the corrosion effects of different anode velocities at a constant current density have been discussed and correlated with varying exposure times. Similarly, the results of various current densities, having been applied to stationary zinc specimens, were analyzed within several current-time product ranges. Results of this latter investigation have provided more knowledge regarding zinc anode

passivation mechanisms. Here, various current-time products indicated that although inception of ZnO platelet nucleation and growth occurs only after a minimum current-time product has been achieved, regardless of the magnitude of either factor within the range examined, the passivating mechanism may be more closely linked to critical values of current density within the product. Figure 65 schematically summarizes the sequence of zinc corrosion under relatively high impressed current densities in a static environment.

D. VELOCITY AND CURRENT DENSITY

The following segment investigates the outcome of combining current densities, in excess of the predetermined galvanic value, with disk speeds greater than 100 rpm over a broad time expanse. In light of the knowledge previously gained by considering each of these factors separately, a more meaningful interpretation of their combined effects should be possible.

At a constant current density of 10 mA/in^2 (1.55 mA/cm^2), the effects of varying anode velocity were significant as was previously reported. When current density was increased by several orders of magnitude during these experiments, the effects of velocity were substantially reduced, both in the laminar and turbulent regimes, and in some cases, it was impossible to deduce, via SEM examination, that the zinc anodes had been rotated. Since corrosion product deposition always depended on the number of zinc ions available, it was logical to expect that if dissolution rates were high enough, a

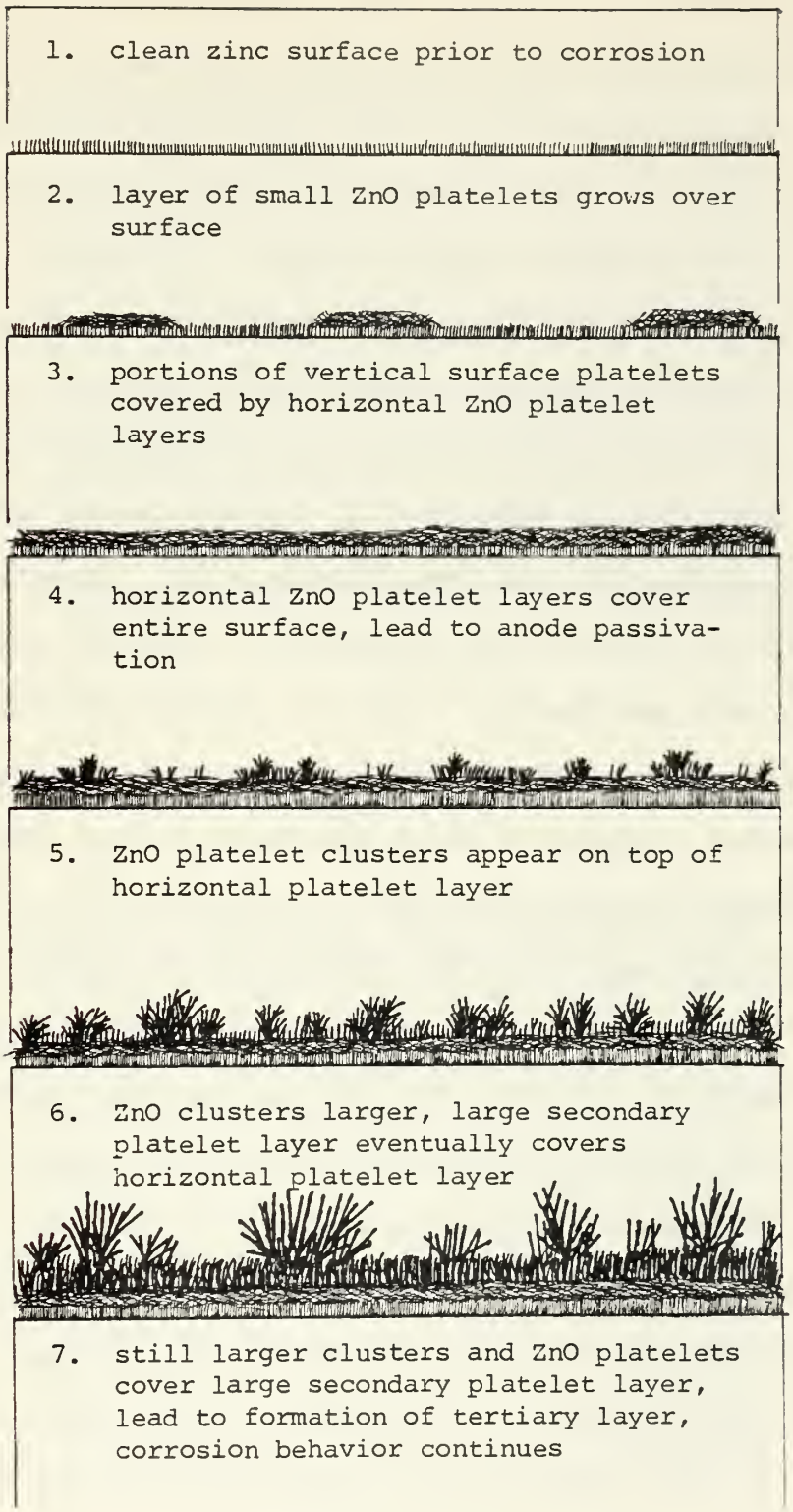

Figure 65

Stationary, long-time exposure of zinc specimen showing effects of increasing current density

sufficient concentration of ions could be provided so as to discount their immediate dispersion into the electrolyte and thus deposition could take place. Such occurrences are compatible with the hydrodynamic and diffusion boundary layer theories. Figures 66, 67, 68, and 69 substantiate this reasoning by illustrating the effects of 200 mA/in^2 (31 mA/cm^2) on specimens rotated at 130 rpm for exposure times of 1,2,5, and 10 minutes respectively. Note that only on the first specimen was there evidence of velocity in the form of a corrosion streak. As reported earlier, ribbonlike structures formed anodic/cathodic interfaces-the enclosed anodic portions showing excessive attack. Figure 70 confirms that in spite of the turbulent velocity field, the electrolyte within the recessed pits became supersaturated to support nucleation and growth of ZnO platelets. With increased exposure time, the pitted regions expanded to eliminate the relatively cathodic areas while platelets rapidly grew in size and number and eventually covered the entire surface. Figures 71 and 72 reveal the extent of a 20 minute corrosive attack on a zinc specimen. The latter figure also shows a secondary layer of network platelets embedded in a cracked compact layer film similar in appearance to that formed on high velocity/low current density specimens. There was no evidence that parts of the cracked film covering were being washed away at this point. The film was remaining anchored and was becoming covered with a secondary platelet network under these conditions.

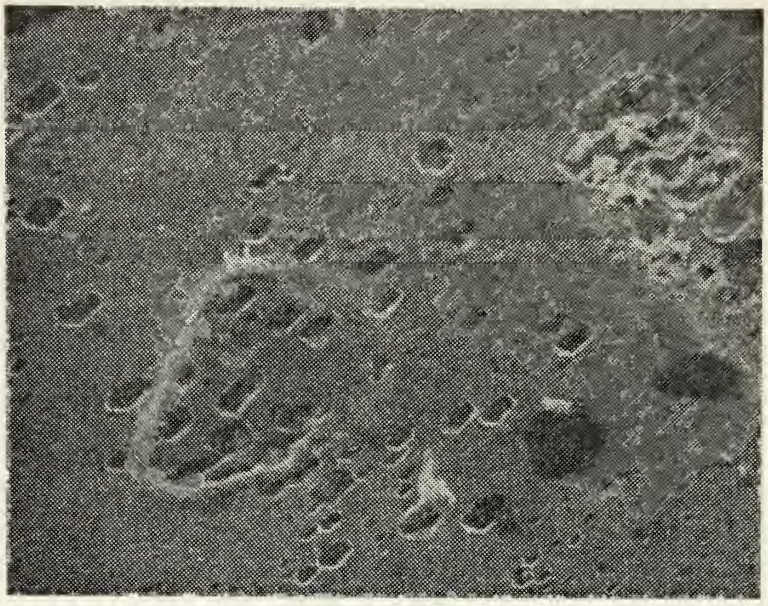

Figure 66

Zinc sample, 1 minute exposure at 200 mA/in^2 (31 mA/cm^2), 130 rpm, 295X (9ES01)

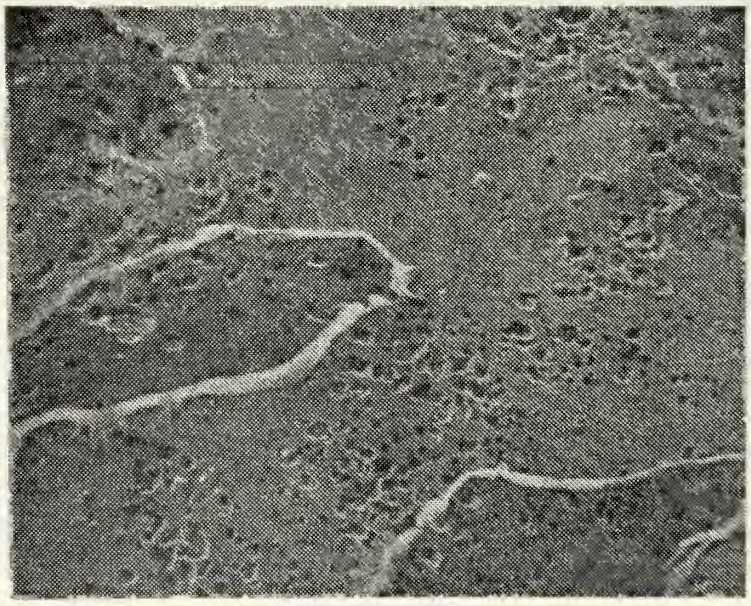

Figure 67

Zinc sample, 2 minute exposure at 200 mA/in^2 (31 mA/cm^2), 130 rpm, 160X (9ES02)

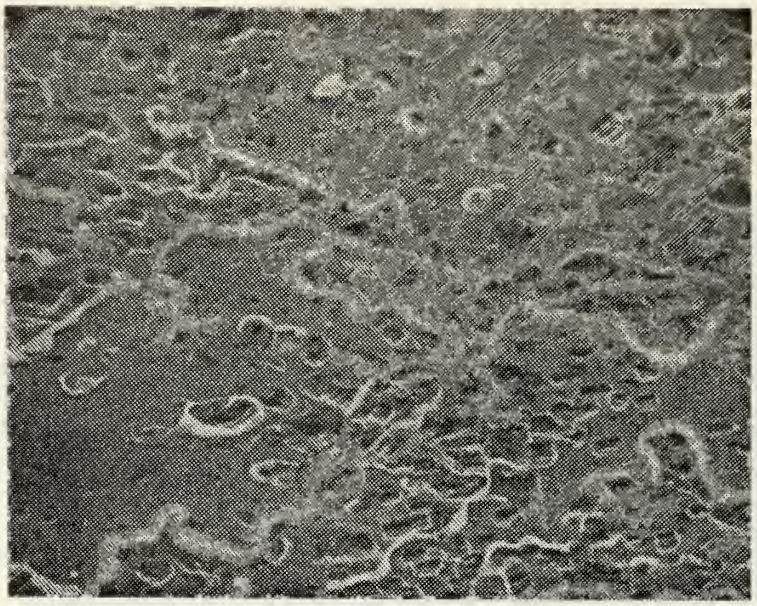

Figure 68

Zinc sample, 5 minute exposure at 200 mA/in^2 (31 mA/cm^2), 130 rpm, 160X (9ES03)

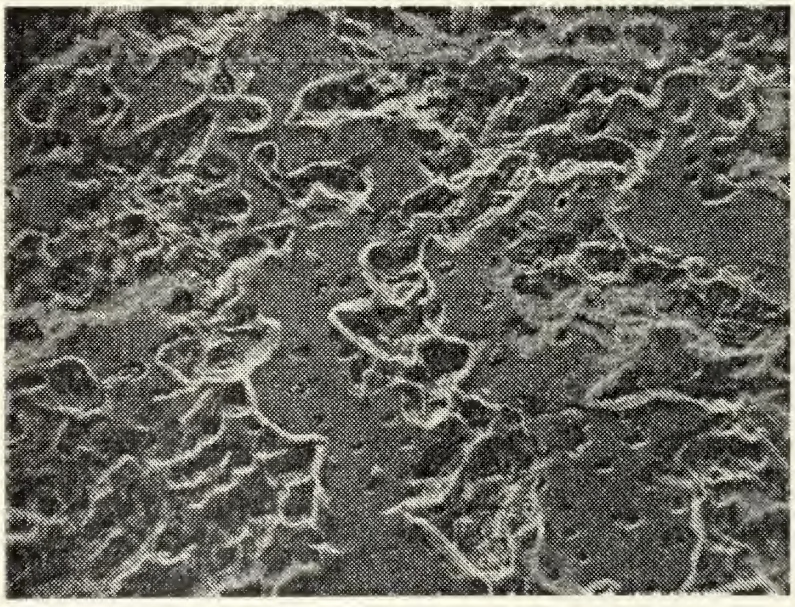

Figure 69

Zinc sample, 10 minute exposure at 200 mA/in^2 (31 mA/cm^2), 130 rpm, 160X (9ES04)

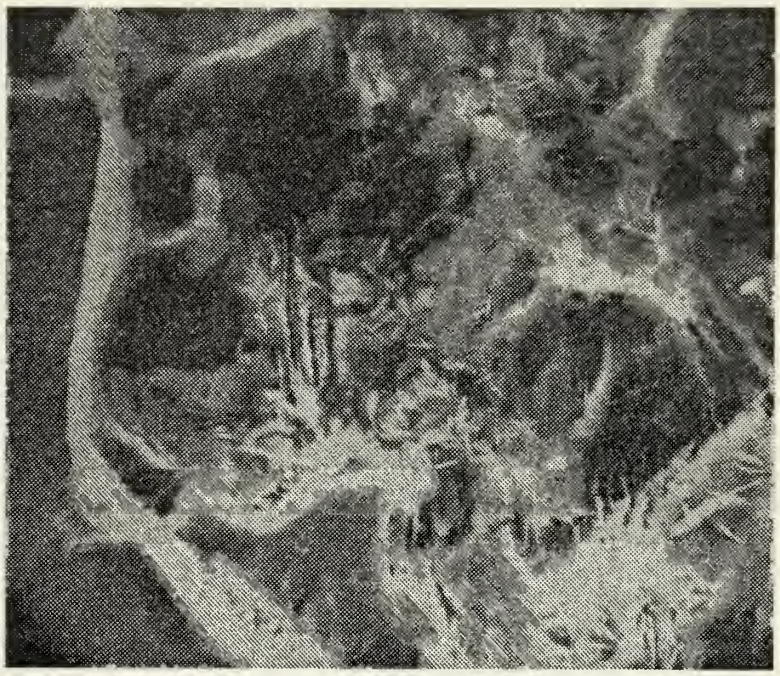

Figure 70

ZnO platelets within pit, zinc sample, 10 minute exposure at 200 mA/in^2 (31 mA/cm^2), 130 rpm, 800X
(9ES04)

Figure 71

Zinc sample, 20 minute exposure at 200 mA/in^2 (31 mA/cm^2), 130 rpm, 160X (9ES05)

Figure 72

Zinc sample, 20 minute exposure at 200 mA/in^2 (31 mA/cm^2), 130 rpm, 750X (9ES05)

Figure 73 exhibits an extremely dense secondary ZnO platelet network growth, which resulted from a 60 minute-200 mA/in^2 (31 mA/cm^2) exposure at 130 rpm. While the specimen was being lightly rinsed with distilled water immediately following the experiment, a clump of the film broke loose and fell from the zinc surface. Figure 74 shows the resulting break away junction while Figure 75 illustrates features on the underlying anode surface. Most interesting is the presence of ribbonlike structures. Observations at short exposure times, discussed earlier, indicated that these ribbon structures might possibly be removed by the electrolyte or "consumed" by ZnO platelet outgrowth. Tilting this specimen within the SEM chamber afforded a sideways view of the film layers remaining on the sample surface, as shown in Figure 76. This angle of examination was unique to this study and provided some interesting information. Most evident in the photograph is the fact that the platelets were embedded in a layer of light, mossy film.

The series of very high current density/high rpm photographs over increasing amounts of exposure time delineates how interactions between these two corrosion factors can vary depending on their relative magnitudes. In this case, velocity effects are shown to be less pronounced on ZnO platelet formation when the extreme current density promotes dense uniform platelet growth. However, this covering does not result in passivation because of its apparent weak attachment to the base metal surface via the mossy film. Figure 77 represents a chronological sequence of sketches depicting

Figure 73

Zinc sample, 60 minute exposure at 200 mA/in^2 (31 mA/cm^2), 130 rpm, 160X (9ES06)

Figure 74

Corrosion product break away junction, zinc sample, 60 minute exposure at 200 mA/in^2 (31 mA/cm^2), 130 rpm, 750X (9ES06)

Figure 75

Uncovered zinc surface, zinc sample, 60 minute exposure at 200 mA/in^2 (31 mA/cm^2) 130 rpm, 300X
(9ES06)

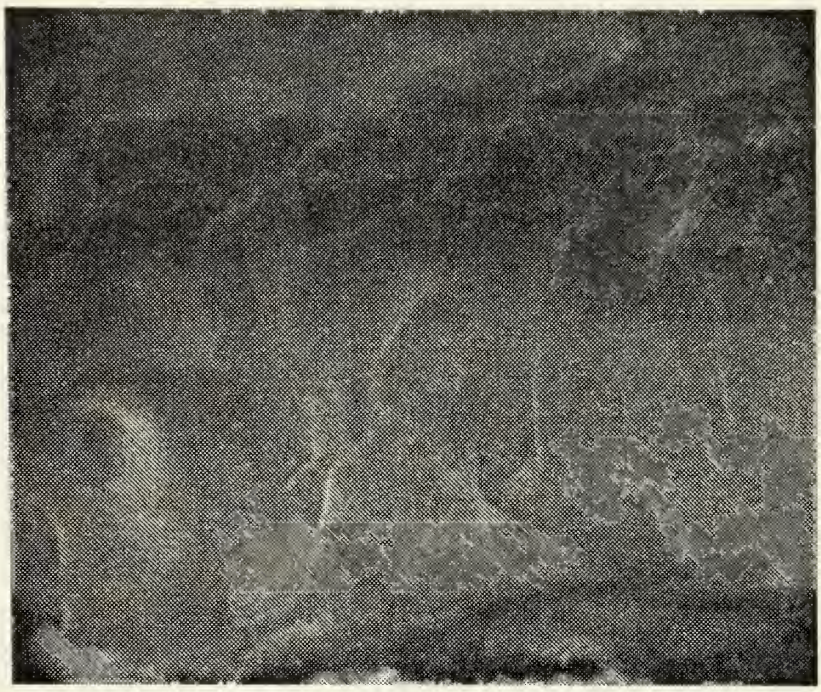

Figure 76

Side view of ZnO platelets embedded in surface film, zinc sample, 60 minute exposure at 200 mA/in^2 (31 mA/cm^2), 130 rpm, 1250X
(9ES06)

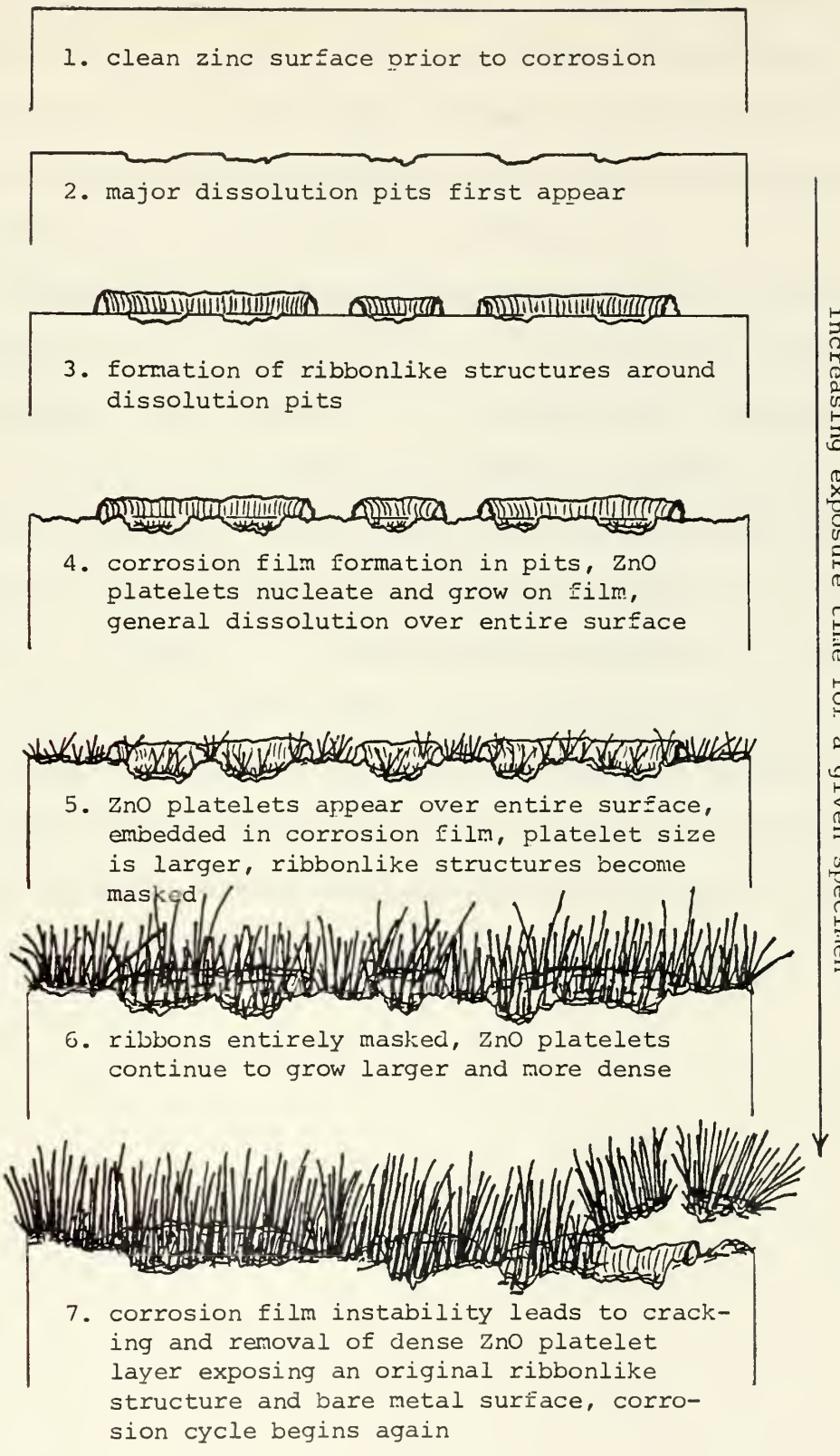

Figure 77

Increasing exposure time of zinc specimen in very-high current density/high velocity environment

corrosion behavior in this situation. These very high current density/high velocity conditions lead to increased film instability and subsequent removal, prior to formation of the secondary platelet network layer seen for lower current density static conditions (see Figure 65).

The information provided by the observations of this study attests to the complexities of the corrosion process and the factors which affect it. The objective throughout this discussion was to single out several corrosion factors considered applicable to the study of galvanic zinc anode passivation and to analyze their probable effects on the phenomenon. Although it would have been possible to conduct several other correlations with the existing data base, such a task was left to future investigators who can benefit by the knowledge gained from this study and use its results to determine optimum experimental schemes with which to explore specific areas of interest.

IV. CONCLUSIONS

The following conclusions have been reached as a direct result of this study:

1. Corrosion of zinc anodes is interdependent on internal (base metal microstructural) and external (electrochemical) variables.

2. Corrosion of zinc anodes is dependent on the external corrosion factors of anodic current density and local velocity environment.

3. Increases in the local velocity, under laminar flow conditions at current densities typical of shipboard galvanic requirements, increases the number of dissolution sites (less corrosive activity per site) as a result of electrical double layer instability. Each dissolution site is trailed by a streak of corrosion product deposition in the direction of local flow.

4. At natural galvanic current densities, turbulent flow conditions give rise to a more compact corrosion product film. A thin layer of electrolyte between this film and the bare metal surface allows nucleation and growth of a fine network of ZnO platelets which in turn gives rise to film cracking and removal. Film formation, cracking, and removal is a cyclical process, which prevents anodic passivation.

5. In a static environment, nucleation and growth of ZnO platelets occurs after a minimum current-time product

exposure of 100 mA•min/in^2 (15.5 mA•min/cm^2).

6. For a given period of time, increasing current density results in more dissolution sites and thus faster and more uniform corrosion product deposition in the absence of velocity effects.

7. Low current density (≈ 10 mA/in^2; 1.55 mA/cm^2)/long time (> 4 hrs) exposures under static conditions can lead to anodic passivation via development of a coherent compact film of ZnO platelets oriented parallel to the anode surface.

8. High current density exposures (above typical galvanic values), i.e., above about 10 mA/in^2 (1.55 mA/cm^2), are not passivating in a stationary environment. The high impressed field promotes growth of primary and secondary platelet networks in a layered fashion, with the outer layer much larger in scale (5 to 10 times the average platelet diameter).

9. As current density increases, the effects of velocity on corrosion product morphology and deposition are diminished. At very high current densities (200 mA/in^2; 31 mA/cm^2) the effects of velocity are nil.

10. Ribbonlike bands of corrosion products define cathodic/anodic interfaces by encircling microanodic areas which may or may not have developed around microcathodic base metal inclusions. These ribbonlike structures appear at current time products less than 100 mA•min/in^2 (15.5 mA•min/cm^2), are usually firmly bonded to the base metal surface, and may become masked by ZnO platelet network overgrowth.

V. RECOMMENDATIONS

The results of this study are a first cut at understanding the important interplay between velocity and current density on the passivation phenomenon of galvanic zinc anodes. Factors of interest in future investigations of these variables should focus on the following considerations:

1. The development of an experimental apparatus in which both the impressed current and the anode/electrolyte velocity can be dealt with in absolute terms should be paramount. Two popular methods currently employed in corrosion research which could be easily adapted to achieve such quantification concerning zinc anodes include: (1) construction of a variable-flow chamber in which electrolyte can be pumped past an array of anodes. Each anode could represent a separate experimental objective designed to examine the individual or combined effects of current density, current-time product, variations in alloying content, temperature, and pH, under various velocity environments. A hot wire anemometer placed in the electrolyte flow would provide accurate determination of its velocity and from this value, hydrodynamic and diffusion boundary layer factors would become more meaningful. (2) use of a small rotating cylindrical anode of sufficient length so that the velocity component effects of its top and bottom surfaces would be insignificant near its central periphery and thus allow accurate determination of relative velocity

in this region prior to post-experimental examination with the SEM. The development of this experimental method would be more feasible than the previously-mentioned method in terms of the time frame allotted to a graduate student.

2. In depth examinations of the effects of very low and very high velocity environments with current density would be useful. (The present study's velocities ranged from approximately 0.75-10 fps (0.29-3.05 m/s) considering disk tangential velocity.)

3. An expanded experimental matrix could be introduced around the current-time product/passivation correlation addressed in this study.

4. A battery of tests should be designed to better simulate shipboard galvanic conditions during which anodes are allowed to corrode under stagnant conditions and are then subjected to a velocity environment or vice versa, prior to SEM examination of surface/corrosion product features.

5. An accurate correlation of anode weight loss with varying velocity and current density combinations should be developed.

Changes in the velocity and current density environment experienced by an active ship's galvanic anodes is commonplace. It is felt that once the dissolution/passivation mechanisms affected by various combinations of these two variables have been properly defined and quantified, a more meaningful investigation of other corrosion factors could be undertaken enroute to the development of improved sacrificial anode systems.

TABLE I

CHEMICAL ANALYSIS OF ZINC SAMPLES*

Metal	% Composition
Cadmium	0.0030
Iron	0.0020
Lead	0.0020
Aluminum	0.0010
Silicon	0.0010
Copper	0.0003
Zinc	Remainder

*Spectrographic analysis by Metallurgical Labs, Inc. San Francisco, California.

TABLE II

MILITARY SPECIFICATION: MIL-A-18001H*
CHEMICAL COMPOSITION REQUIREMENTS, ZINC ANODES

Metal		% Composition
Cadmium	(range)	0.025-0.15
Iron	(maximum)	0.005
Lead	(maximum)	0.006
Aluminum	(range)	0.10-0.50
Silicon	(maximum)	0.125
Copper	(maximum)	0.005
Zinc		Remainder

*MIL-A-18001H [5].

TABLE III

EXPERIMENTAL PARAMETERS**

EXPERIMENT #1:

SPECIMEN	CURRENT DENSITY mA/in^2	mA/cm^2	EXPOSURE TIME Minutes	DISK RPM
1ES01	5	0.775	5	15
1ES02	5	0.775	10	15
1ES03	5	0.775	20	15
1ES04	10	1.550	10	15
1ES05	10	1.550	20	15
1ES06	10	1.550	40	15
1ES07	20	3.100	20	15

Conductivity: 42.0 mmho
pH : 8.1

EXPERIMENT #2:

2ES01	5	0.775	1	15

Conductivity: 42.0 mmho
pH : 8.1

EXPERIMENT #3:

3ES01	10	1.550	40	10
3ES02	10	1.550	40	30
3ES03	10	1.550	40	45
3ES04	10	1.550	40	60
3ES05	10	1.550	40	75
3ES06	10	1.550	40	90
3ES07	10	1.550	40	105
3ES08	10	1.550	40	120
3ES09	10	1.550	40	200

Conductivity: 44.0 mmho
pH : 8.3

EXPERIMENT #4:

SPECIMEN	CURRENT DENSITY mA/in^2	mA/cm^2	EXPOSURE TIME Minutes	DISK RPM
4ES01	10	1.550	40	30
4ES02*	10	1.550	40	30

*Man-made pits and scratches on surface
Conductivity: 42.0 mmho
pH : 8.35

EXPERIMENT #5:

5ES01	10	1.550	40	0
5ES02	10	1.550	40	30

Conductivity: 42.5 mmho
pH : 8.2

EXPERIMENT #6:

6ES01	5	0.7750	2	0
6ES02	5	0.7750	3	0
6ES03	5	0.7750	4	0
6ES04	5	0.7750	5	0
6ES05	1	0.1550	2	0
6ES06	1	0.1550	5	0
6ES07	0.5	0.0775	2	0
6ES08	0.5	0.0775	10	0
6ES09	0.5	0.0775	30	0

Conductivity: 43.0 mmho
pH : 8.2

EXPERIMENT #7:

7ES01	50	7.750	40	0
7ES02	50	7.750	120	0
7ES03	50	7.750	8	0
7ES04	50	7.750	2	0
7ES05	10	1.550	240	0
7ES06	10	1.550	240	130
7ES07	10	1.550	240	50

Conductivity: 41.5 mmho
pH : 8.2

SPECIMEN	CURRENT DENSITY mA/in^2	mA/cm^2	EXPOSURE TIME Minutes	DISK RPM
EXPERIMENT #8:				
8ES01	5	0.775	240	0
8ES02	20	3.100	240	0
8ES03	30	4.650	240	0
8ES04	38	5.890	240	0
8ES05	50	7.750	240	0
8ES06	20	3.100	900	0
Conductivity:	44.5 mmho			
pH :	8.3			
EXPERIMENT #9:				
9ES01	200	31	1	130
9ES02	200	31	2	130
9ES03	200	31	5	130
9ES04	200	31	10	130
9ES05	200	31	20	130
9ES06	200	31	60	130
9ES07	200	31	10	40
9ES08	100	15.50	10	40
9ES09	10	1.550	10	40
9ES10	10	1.550	240	30
9ES11	10	1.550	240	130
Conductivity:	43.5 mmho			
pH :	8.3			

**All experiments performed at room temperature, approximately 77°F (25°C).

APPENDIX A

PREPARATION OF ARTIFICIAL SEAWATER

Synthetic standard seawater required during experimentation was prepared using the formula and procedure developed by Kester et al [23]. A concentrated stock solution was initially produced for ease in handling prior to use.

The following amounts of gravimetric and volumetric salts, combined with enough distilled water for a total weight of 1 kilogram, were used per kilogram of synthetic seawater solution.

A. Gravimetric Salts

salt	g/kg of solution
NaCl	23.926
Na_2SO_4	4.008
KCl	0.677
$NaHCO_3$	0.196
KBr	0.098
H_3BO_3	0.026
NaF	0.003

B. Volumetric Salts

salt	Conc M/L	ml/kg of solution
$MgCl_2 \cdot 6H_2O$	1.000	53.27
$CaCl_2 \cdot 2H_2O$	1.000	10.33
$SrCl_2 \cdot 6H_2O$	0.100	0.90

C. Distilled water to bring total weight to 1 kilogram

The following is a comparison of the composition of natural and artificial seawaters by their ionic content.

Ion	Natural Seawater (g/kg)	Artificial Seawater (g/kg)	Difference %
Cl^-	19.353	19.353	0.0
Na^+	10.760	10.765	0.046
SO_4^{--}	2.712	2.711	0.037
Mg^{++}	1.294	1.295	0.077
Ca^{++}	0.413	0.414	0.24
K^+	0.387	0.387	0.0
HCO_3^-	0.142	0.142	0.0
Br^-	0.067	0.066	1.5
H_3BO_3	0.026	0.026	0.0
Sr^{--}	0.008	0.008	0.0
F^-	0.001	0.001	0.0

APPENDIX B

The following discussion addresses features and operating characteristics of the current generator/power source used in experimentation and was written by the designer of the apparatus.

VOLTAGE CONTROLLED CURRENT GENERATOR AND VOLTAGE CONTROLLED VOLTAGE GENERATOR

Tom Christian
Department of Mechanical Engineering
Naval Postgraduate School
Monterey, California

This device consists of two separate voltage-regulated supplies which share a common, raw, 24 volt D.C. source. The two sources may not be coupled in series or parallel.

The Voltage Controlled Voltage Generator is a fairly simple power supply consisting of a positive voltage regulator (LM-723) with an outboard pass transistor and current limiting network providing a regulated D.C. voltage of approximately +1.5 volts to +30.0 volts at currents of up to 1 ampere. This configuration yields regulation of nominally 1% and is intended to drive small motors.

The Voltage Controlled Current Generator provides a regulated current of up to 0.750 amperes depending upon the position of the range switch. The device will source whatever current is necessary from the CURRENT SOURCE port through the external load and into the CURRENT RETURN port, in order to keep the selected voltage constant across the RANGE resistor.

The control voltage may be varied from +0.80 volts to +7.50 volts. This voltage across the range resistor according to OHM'S LAW will determine the current.

Since the load is in series with the RANGE resistor and current is the same in all parts of a series circuit (KIRCHOFF'S LAW), the current is controlled by the E/R relationship. The dynamic response of this configuration is on the order of 15 microseconds and overall regulation is 0.1% of full scale of the selected range.

Inasmuch as a potential must be established across the load in order to provide a current, the VCCG does have a finite limit as to how much current it can effectively source. To alert the operator when the limits are being approached, a LIGHT EMITTING DIODE is incorporated in the circuit. A voltage comparator (½747) activates the LED when the output voltage is 90% of the available, raw D.C. voltage. When this condition exists, current regulation cannot be maintained.

For convenience, an identical comparator (½747),LED, and associated network is incorporated in the VCCG to warn the operator that voltage regulation cannot be maintained.

LIST OF REFERENCES

1. Uhlig, H. H., Corrosion and Corrosion Control, John Wiley & Sons, Inc., p. 20-214, 1971.

2. Henthorne, M., Fundamentals of Corrosion, Chemical Engineering, a series of articles, (5/17/71-4/3/72).

3. Davy, H., "On the Corrosion of Copper Sheathing on Ships by Seawater, and a Method of Preventing This Effect; and in Their Application to Ships of War and Other Ships," Phil. Trans. Roy. Soc. (London), 1824; Corrosion, 3, 295, 1947.

4. Teel, R. B. and Anderson, D. B., "The Effect of Iron in Galvanic Zinc Anodes in Sea Water," Corrosion, v. 12, p. 53-59, 1956.

5. Military Specifications MIL-A-18001H, Anodes, Corrosion Prevention, Zinc; Slab, Disc, and Rod Shaped, 28 June 1968.

6. Francis, R. C. and Cook, F. E., "Economics of Cathodic Protection for U. S. Navy Ships," Materials Protection, v. 1, no. 2, p. 18-20; 22-23, 1962.

7. Birnbaum, L., Taylor B., Strasburg, W., "Cathodic Protection," Naval Engineers Journal, April 1971, p. 13-24, April 1971.

8. Tomashov, N. D., Theory of Corrosion and Protection of Metals, The Macmillan Company, p. 271-324; 454-481, 1966.

9. Fontana, M. Greene N., Corrosion Engineering, McGraw-Hill Book Company, p. 76-78; 104-106; 299-305; 310-312; 76-78; 1967.

10. Bosich, J. F., Corrosion Prevention for Practicing Engineers, Barnes & Noble, p. 43, 1970.

11. Monney, N. T., "Deep Ocean Corrosion-Simulation Facilities vs. In-Situ Research," Materials Protection and Performance, v. 12, no. 1, p. 10-13, Jan. 1973.

12. Teel, R. B. and Anderson, D. B., "The Effect of Minor Elements on the Current Output Characteristics of Zinc Galvanic Anodes in Sea Water," Navy-Industry Zinc Symposium on Cathodic Protection, April 1955, Bureau of Ships, Navy Dept., Washington.

13. Reichard, E. C., and Lennox, T. J., "Shipboard Evaluation of Zinc Galvanic Anodes Showing the Effect of Iron, Aluminum, and Cadmium on Anode Performance," Corrosion, v. 13, p. 410-416, 1957.

14. Carson, J.A.H., "Zinc as a Self-Regulating Galvanic Anode for Ship Hulls," Corrosion,v. 16, p. 491-496, 1960.

15. Carson, J., Phillips, W. and Wellington, J., "A Laboratory Evaluation of Zinc Anodes in Sea Water," Corrosion, v. 16, p. 171-177, 1960.

16. Waldron, L. J., and Peterson, M. H., "Effect of Iron, Aluminum, and Cadmium Additions on the Performance of Zinc Anodes in Sea Water," Corrosion, v. 16, p. 375-379, 1960.

17. Southin, R. T., "Some Observations on the Microstructure of Zinc Alloy Anodes," J. Inst. Metals, v. 93, p. 428-431, 1964-65.

18. Gliszewski, L., and Malinowski, S., "A Study of Zinc Anode Behavior in Sea Water," Proceedings of the 4th Int. Cong. on Metallic Corrosion, NACE, p. 714-715, 1972.

19. Bornholdt, R. A., and Perkins, A. J., "SEM Examinations of Corrosion Product Morphology for Anodically Polarized Zinc," Metallography, v. 8, p. 39-47, 1975.

20. Todd, J. M., and Perkins, A. J., "Corrosion of Zinc Anodes in Seawater," Naval Engineers Journal, (in press, 1976).

21. Todd, J. M., and Perkins, A. J., "Nucleation and Growth of Anodic Electrocrystallization Products on Zinc in Saltwater Solutions," Corrosion, (in press, 1976).

22. Todd, J. M., Nucleation and Growth of Anodic Electrocrystallized Products on Ship Hull Zinc in Salt Water Solutions, MSME-Mechanical Engineer Thesis, Naval Postgraduate School, December 1975.

23. Kester, D. R., Duedall, I. W., Conners, D. N., and Pytkowicz, R. M., "Preparation of Artificial Seawater," Limnology and Oceanography, v. 12, p. 176-178, Dec. 1967.

24. Petrocelli, J. V., "Electrochemistry of Dissolution Processes," The Surface Chemistry of Metals and Semiconductors, H. Gatos, editor, p. 326-356, 1960.

25. White, R., Mohr, C. and Newman, J., "The Fluid Motion Due to a Rotating Disk," Journal of the Electrochemical Society, v. 123, no. 3, March 1976.

26. Gerischer, H., "Metal and Semiconductor Electrode Processes," The Surface Chemistry of Metals and Semiconductors, H. Gatos, editor, p. 177-204, 1960.

27. Farmer, E. D., and Webb, A. H., "Zinc Passivation and the Effect of Mass Transfer in Flowing Electrolyte," Journal of Applied Electrochemistry, v. 2, p. 123-139, 1972.

28. Private communication with Professor Turgut Sarpkaya at the Naval Postgraduate School, March 1976.

29. Powers, R. W. and Breiter, M. W., "The Anodic Dissolution and Passivation of Zinc in Concentrated Potassium Hydroxide Solutions," Journal of the Electrochemical Society, v. 116, no. 6, p. 719-728, 1969.

30. Powers, R. W., "Anodic Films on Zinc and the Formation of Cobwebs," Journal of the Electrochemical Society, v. 116, no. 12, p. 1652-1659, 1969.

31. Hull, M., Ellison, Y., and Toni, J., "The Anodic Behavior of Zinc Electrodes in Potassium Hydroxide Electrolytes," Journal of the Electrochemical Society, v. 117, no. 2, p. 192-197, 1970.

32. Powers, R. W., "Film Formation and Hydrogen Evolution on the Alkaline Zinc Electrode," Journal of the Electrochemical Society, v. 118, no. 5, p. 685-695, 1971.

33. Conway, B. E., Theory and Principles of Electrode Processes, The Ronald Press Company, p. 200-201, 1965.

INITIAL DISTRIBUTION LIST

		No. Copies
1.	Defense Documentation Center Cameron Station Alexandria, Virginia 22314	2
2.	Library, Code 0212 Naval Postgraduate School Monterey, California 93940	2
3.	Department Chairman, Code 59 Department of Mechanical Engineering Naval Postgraduate School Monterey, California 93940	2
4.	Professor A. J. Perkins, Code 59Ps Department of Mechanical Engineering Naval Postgraduate School Monterey, California 93940	5
5.	Professor T. Sarpkaya, Code 59Sl Department of Mechanical Engineering Naval Postgraduate School Monterey, California 93940	1
6.	Professor D. Salinas, Code 59Zc Department of Mechanical Engineering Naval Postgraduate School Monterey, California 93940	1
7.	Mr. Tom Christian, Code 59 Department of Mechanical Engineering Naval Postgraduate School Monterey, California 93940	1
8.	Mr. George Bixler, Code 59 Department of Mechanical Engineering Naval Postgraduate School Monterey, California 93940	1
9.	ENS William Howard Luebke, USN P. O. Box 871 Lake City, Florida 32055	5

10. Capt. Dean Taylor 1
Chief of Staff
Naval Postgraduate School
Monterey, California 93940

11. LT Pete Wright 1
Department of Mechanical Engineering
Naval Postgraduate School
Monterey, California 93940

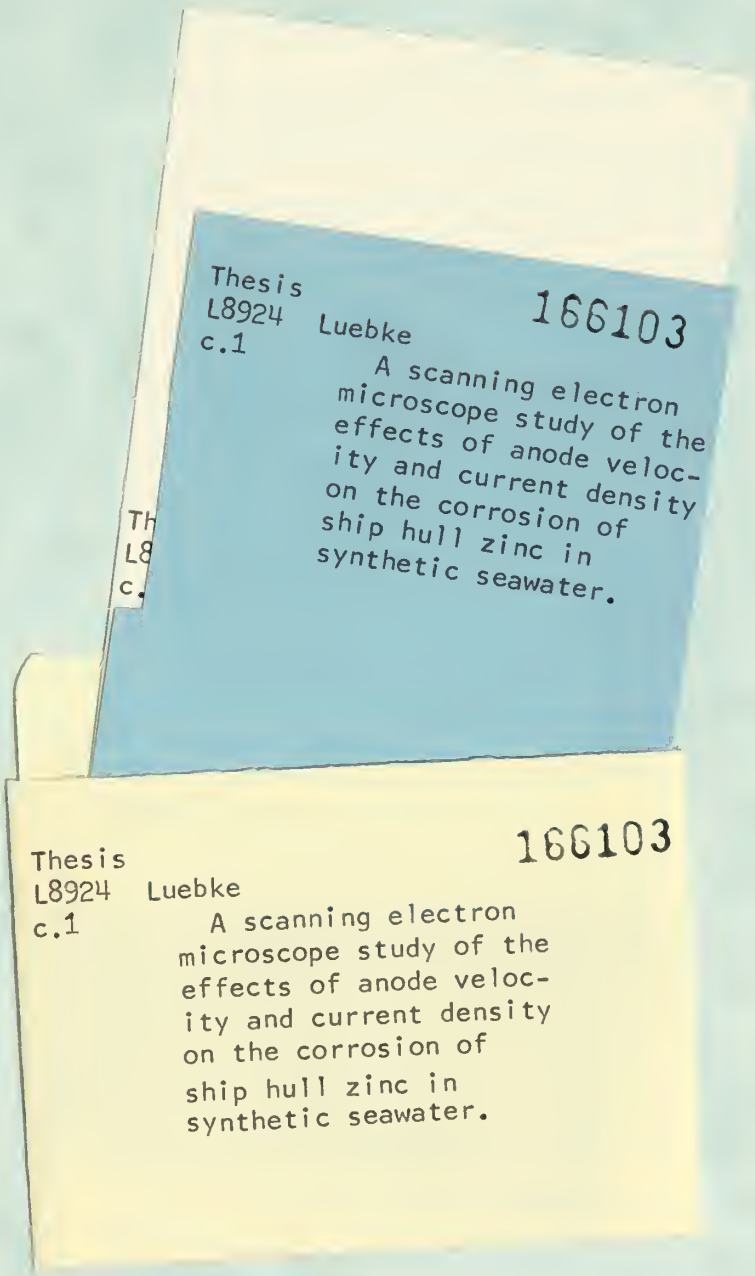
Thesis
L8924
c.1
Luebke
166103
A scanning electron microscope study of the effects of anode velocity and current density on the corrosion of ship hull zinc in synthetic seawater.
Thesis
L8924
c.1
Luebke
166103
A scanning electron microscope study of the effects of anode velocity and current density on the corrosion of ship hull zinc in synthetic seawater.